

Halo Model Analysis of Cluster Statistics

Eduardo Rozo^{1,2}, Scott Dodelson^{3,4}, Joshua A. Frieman^{2,3,4}

¹*Dept. of Physics, The University of Chicago, Chicago, IL 60637*

²*Center for Cosmological Physics, Chicago, IL 60637*

³*NASA/Fermilab Astrophysics Center Fermi National Accelerator Laboratory, Batavia, IL 60510 and*

⁴*Dept. of Astronomy and Astrophysics, The University of Chicago, Chicago, IL 60637*

We use the halo model formalism to provide expressions for cluster abundances and bias, as well as estimates for the correlation matrix between these observables. Off-diagonal elements due to scatter in the mass tracer scaling with mass are included, as are observational effects such as biases/scatter in the data, detection rates (completeness), and false detections (purity). We apply the formalism to a hypothetical volume limited optical survey where the cluster mass tracer is chosen to be the number of satellite galaxies assigned to a cluster. Such a survey can strongly constrain σ_8 ($\Delta\sigma_8 \approx 0.05$), the power law index α where $\langle N_{gal}|m \rangle = (m/M_1)^\alpha$ ($\Delta\alpha \approx 0.03$), and perhaps even the Hubble parameter ($\Delta h \approx 0.07$). We find cluster abundances and bias are not well suited for constraining Ω_m or the amplitude M_1 . We also find that without bias information σ_8 and α are degenerate, implying constraints on the former are strongly dependent on priors used for the latter and vice-versa. The degeneracy stems from an intrinsic scaling relation of the halo mass function, and hence it should be present regardless of the mass tracer used in the survey.

I. INTRODUCTION

Two of the simplest measures of how matter is distributed throughout the universe are its average density, parametrized by the ratio of the matter density to the critical density, Ω_m , and its power spectrum $P(k)$. The amplitude of the power spectrum today is usually characterized by σ_8 , the average rms mass fluctuation in spheres of $8h^{-1}\text{Mpc}$. Accurate determinations of both σ_8 and Ω_m are of crucial importance to cosmology as they provide some of the simplest probes of large scale structure.

Cluster abundances are well known for their ability to constrain both σ_8 and Ω_m (see e.g. [40],[53], [1],[24],[39],[52], [29],[4], [45] and references therein). This seems intuitively reasonable: the number of large massive objects ought to depend on the total mass available (Ω_m) and a measure of how likely is it for mass to clump at cluster scales (σ_8). More formally, from numerical simulations ([26],[17]) and theoretical considerations ([41], [43]) we know to a reasonable accuracy what the halo mass function looks like in various cosmologies. Even though mass is not directly observable, by identifying a mass tracer and its relation to halo mass one may hope to constrain cosmology. Some examples of mass tracers in clusters are X-ray temperatures and luminosities of the inter-cluster gas, optical luminosities, and the number of galaxies found in the cluster.

The actual analysis of data may be quite involved. In particular, not only is it necessary to understand how a mass tracer scales with halo mass, one also needs to understand both what the uncertainties in the scaling are and the intrinsic scatter around the mean relation between the mass tracer and halo mass (see e.g. Pierpaoli et al. [40], Viana et al. [53] for two recent, detailed analyses).

Here, we develop simple expressions for the number density and bias of clusters binned using an arbitrary mass tracer. While much effort has been devoted to converting observations to the theoretically simple mass function, here we attempt to massage the theory to fit the observations: i.e. use the halo model to make predictions for any experiment. We attempt to include many of the most relevant experimental effects, including intrinsic scatter in the mass tracer, scatter and/or bias arising from experimental measurements, and imperfect detection rates and false detections. We feel this is important since it allows direct comparison of theory to data: by minimizing the amount of data manipulation, the probability of artificially biasing the data is diminished.

We also provide theoretical estimates of the correlation matrix between various bins. Our estimates include Poisson noise, sample variance, and uncertainties due to scatter in the scaling of the mass tracer with mass, the treatment of which we believe is new.

Following the development of our formalism, we apply it to a model cluster catalogue that mimics the type of catalogues one can construct from large optical surveys such as the SDSS [55] or the 2dF [13]. For concreteness, we take the mass tracer to be the number of member galaxies in a cluster. This has the interesting consequence that we can analyze both cosmological constraints and constraints on how galaxies populate halos.

From the cosmological point of view, our results are of importance since any new measurements of σ_8 may help narrow the large range of measured values for this quantity. More importantly perhaps, our analysis identifies degeneracies between cosmology and the halo occupation distribution. Not only is this an interesting problem in itself

(see e.g. Zheng et al. [57], Berlind & Weinberg [8]), but the identification of degeneracies in our survey suggests that, in general, there will be degeneracies between cosmology and the mass tracer scaling relation. Said degeneracies may help bring into agreement seemingly conflicting results for σ_8 obtained with different assumptions of the mass tracer scaling relation.

From the point of view of constraining galaxy formation, determining both cosmology and the halo occupation distribution simultaneously is important since it avoids possible systematic errors that may arise from the choice of an incorrect cosmology (again coming back to the question of degeneracies). Further, we believe that considering cluster abundances and large scale bias has the important advantage that neither halo profiles nor second order moments of the halo occupation distribution appear in our formulae explicitly. This makes our results very insensitive to said variables, thereby providing a first stepping stone toward the full determination of the halo occupation distribution. In particular, this type of analysis should complement well halo occupation constraints from galaxy clustering (see e.g. Jing, Mo, and Börner [27], Scoccimarro et al. [46], Moustakas and Somerville [35], Cooray [14]), as well as more sophisticated studies of halo occupancy such as work based on the conditional luminosity function (see Yang, Mo and van den Bosch [54] and van den Bosch, Mo, and Yang [51]).

In section 2, we develop our formalism and find expressions for the number density and bias of clusters binned according to measurements of an arbitrary mass tracer. In section 3 we identify the various sources of uncertainty intrinsic to observations, i.e. uncertainties that would exist even for a perfect experiment. In section 4, we show how to include various experimental effects both in the predictions for what will be observed and in the uncertainties associated with the data. Having finished our formalism, we present in section 5 the assumptions for our model survey and characteristics of the assumed cluster catalogue. These are supposed to mimic the real catalogues which one may expect to construct with surveys such as the SDSS and 2dF. Section 5 sets up our fiducial model and states all assumptions used to obtain our results, which are presented in section 6. Section 7 addresses how the results change if we do not have bias information and consider cluster abundances alone. We present our conclusions in section 8. Also included as an appendix is a more thorough discussion of what is usually called the cluster abundance normalization condition ($\sigma_8\Omega_m^\gamma \approx 0.5$, $\gamma \approx 0.5$) than the one presented in the main text.

II. HALO MODEL FORMALISM AND CLUSTER STATISTICS:

A. The Halo Model Approach

The Halo Model is a theoretical framework developed to understand clustering properties of different mass tracers in the universe. The halo model does this by dividing the problem in two: first, it assumes all mass in the universe is distributed in units called halos. The halo model then assumes that all properties of mass tracers within a halo (e.g. galaxies, X-ray temperature, etc.) are determined exclusively by the physical properties of the parent halo (e.g. mass, angular momentum, and so on).¹

Let then η be our mass tracer, e.g. X-ray temperature/luminosity, optical luminosity, or number of member galaxies. We will be interested in the clustering properties of halos as a function of the tracer η . In particular, we will be interested in the density and bias of halos for an arbitrary binning criterion $\psi(\eta)$. For instance, one may wish to bin clusters by specifying the maximum and minimum values η may take for a cluster to be included in a specific bin. This corresponds to a top-hat selection function $\psi(\eta) = 1$ when $\eta_{max} > \eta \geq \eta_{min}$ and $\psi(\eta) = 0$ otherwise. Since we will be interested in medium and large mass halos, we will be using the terms halos, groups, and clusters interchangeably.

B. Cluster Density

Let us write then the cluster density in the halo model formalism. Let the i^{th} halo be located at position \vec{x}_i and let η_i be the value of the mass tracer η for that particular halo. Then the density of objects where η is larger than some specified minimum value η_{min} is given by

$$n_{cl}(\vec{x}) = \sum_i \delta(\vec{x} - \vec{x}_i) \theta(\eta_i - \eta_{min}) \quad (1)$$

¹ In the simplest cases, halos are taken to be spherical distributions of dark matter, with some specified density profile, typically an NFW [36] or Moore [34] profile. For our purposes, neither the shape nor the mass distribution of the halos will be important.

where the sum is over all halos. Here, $\theta(x)$ is the usual step function, i.e. $\theta(x) = 1$ for $x \geq 0$ and $\theta(x) = 0$ otherwise, so that a halo contributes to the density if and only if $\eta \geq \eta_{min}$. Alternatively, one may be interested in some other selection criteria, e.g. looking at objects with $\eta_{max} > \eta \geq \eta_{min}$, characterized by a top-hat function as discussed above. Let $\psi_{\vec{a}}(\eta)$ represent an arbitrary window function used to bin data, where \vec{a} contains the parameters that specify the binning. In this case, the above expression becomes

$$n_{\vec{a}}^t(\vec{x}) = \sum_i \delta(\vec{x} - \vec{x}_i) \psi_{\vec{a}}(\eta_i) \quad (2)$$

where the superscript t is meant to signify that this is the true density of objects in our bin: i.e what we would observe with perfect instruments. Systematic effects brought about by observations may lead to an observed density $n_{\vec{a}} \neq n_{\vec{a}}^t$. We fold these into our formalism in §4.

We now make use of the ergodic hypothesis, and assume that the spatial clustering statistics of any field are identical to those obtained upon averaging the corresponding expressions over a hypothetical ensemble of universes. Using $\langle \rangle$ to denote ensemble average, and an over bar $\bar{}$ to denote spatial averaging, we expect the spatially averaged cluster density to be:

$$\bar{n}_{\vec{a}}^t = \langle \sum_i \delta(\vec{x} - \vec{x}_i) \psi_{\vec{a}}(\eta_i) \rangle \quad (3)$$

In order to obtain expectation values, one needs to know then the probability distribution for η_i . We make the standard assumption that the value of the observable η for a halo of mass m is a random variable with a probability distribution $P(\eta|m)$ depending only on the mass m of the halo. For instance, the assumption of hydrostatic equilibrium in clusters allows one to relate the observed X-ray temperature to the mass of the cluster. Likewise, simulations seem to indicate that the number of galaxies N in a halo of mass m is relatively insensitive to environment, so that $P(N)$ depends only on m [9],[32].

Writing $\eta_i = \eta(m_i)$, where η is a random variable for each mass value m_i , we can rewrite the expression above as:

$$\begin{aligned} \bar{n}_{\vec{a}}^t &= \left\langle \sum_i \delta(\vec{x} - \vec{x}_i) \psi_{\vec{a}}(\eta(m_i)) \right\rangle \\ &= \int_0^\infty dm \left\langle \sum_i \delta(m - m_i) \delta(\vec{x} - \vec{x}_i) \psi_{\vec{a}}(\eta(m)) \right\rangle \\ &= \int_0^\infty dm \left\langle \sum_i \delta(m - m_i) \delta(\vec{x} - \vec{x}_i) \right\rangle \langle \psi_{\vec{a}}(\eta(m)) \rangle. \end{aligned}$$

Notice that is only because we are assuming that η is independent of cosmology that we can take $\psi_{\vec{a}}(\eta(m))$ out of the ensemble average above, and consider its average value over the halo occupation distribution alone.² We now define the quantity

$$n(m, \vec{x}) \equiv \sum_i \delta(m - m_i) \delta(\vec{x} - \vec{x}_i), \quad (4)$$

which represents the true halo density field, the spatial average of which is called the halo mass function $\bar{n}(m)$. We obtain then that the number density of groups in a bin \vec{a} is

$$\begin{aligned} \bar{n}_{\vec{a}}^t &= \int_0^\infty dm \langle n(m, \vec{x}) \rangle \langle \psi_{\vec{a}}(\eta(m)) \rangle \\ &= \int_0^\infty dm \bar{n}(m) \langle \psi_{\vec{a}}|m \rangle. \end{aligned} \quad (5)$$

where $\langle \psi_{\vec{a}}|m \rangle$ is meant to be the average value of $\psi_{\vec{a}}(\eta(m))$ over the probability distribution $P(\eta|m)$.

² This is a crucial and strong assumption. In particular, any dependence of the chosen mass tracer on the large scale environment would bias our results.

C. The Cluster-Cluster Correlation Function and Power Spectrum

Following an argument similar to the one above we may obtain an expression for the cluster-cluster correlation function $\xi_{\vec{a},\vec{a}'}^t(r)$ between objects in bins \vec{a} and \vec{a}' (here $r = |\vec{x} - \vec{x}'|$):

$$\begin{aligned}\xi_{\vec{a},\vec{a}'}^t(r) &= \langle (\frac{n_{\vec{a}}^t(\vec{x})}{\bar{n}_{\vec{a}}^t} - 1)(\frac{n_{\vec{a}'}^t(\vec{x}')}{\bar{n}_{\vec{a}'}^t} - 1) \rangle \\ &= -1 + \int_0^\infty dm dm' \langle \psi_{\vec{a}} | m \rangle \langle \psi_{\vec{a}'} | m' \rangle \frac{\langle n(m, \vec{x}) n(m', \vec{x}') \rangle}{\bar{n}_{\vec{a}}^t \bar{n}_{\vec{a}'}^t} \\ &= -1 + \int_0^\infty dm dm' \langle \psi_{\vec{a}} | m \rangle \langle \psi_{\vec{a}'} | m' \rangle \frac{\bar{n}(m) \bar{n}(m')}{\bar{n}_{\vec{a}}^t \bar{n}_{\vec{a}'}^t} (1 + \xi_{hh}(r|m, m')) \\ &= \int dm dm' \xi_{hh}(r|m, m') \langle \psi_{\vec{a}} | m \rangle \langle \psi_{\vec{a}'} | m' \rangle \frac{\bar{n}(m) \bar{n}(m')}{\bar{n}_{\vec{a}}^t \bar{n}_{\vec{a}'}^t}\end{aligned}$$

where $\xi_{hh}(r|m, m')$ is the halo correlation function between halos of different masses m and m' separated by distance r . The upper script t on $\xi_{\vec{a},\vec{a}'}^t$ serves here again to remind us that this is the true cluster correlation function. The observed correlation function may differ from $\xi_{\vec{a},\vec{a}'}^t$ due to systematics effects in the observations, to be included later. From our discussion concerning the average cluster density, we already know how to handle $\bar{\psi}_{\vec{a}}(m)$ and $\bar{n}(m)$. The only term in the above expression which is new is ξ_{hh} .

The halo model provides a prescription to relate δ_h , the halo overdensity, to the matter overdensity. This same prescription relates the halo correlation function to the linear correlation function. To first order in perturbation theory, one obtains (see e.g. [15], [43]) $\delta_h = \bar{b}(m) \delta_m^{\text{lin}}$ where

$$\begin{aligned}\bar{b}(m) &= 1 - \frac{\partial \ln \bar{n}(m)}{\partial \delta_{sc}} \\ &= 1 + \frac{q\nu - 1}{\delta_{sc}} + \frac{2p}{\delta_{sc}(1 + (q\nu)^p)}\end{aligned}\tag{6}$$

is the linear bias [43]³. Here δ_{sc} is the critical overdensity needed for collapse, $\delta_{sc} = 1.686$; $q = 0.75$ and $p = 0.3$ come from fitting to N -body simulations; and $\nu \equiv \delta_{sc}^2 / \sigma_{\text{lin}}^2(m)$, with σ_{lin} being the tophat filtered rms fluctuations in the linear density field. The radius R of the top-hat filter used in defining $\sigma(m)$ is obtained by demanding that a sphere of radius R encompasses a total mass m , i.e. $\Omega_m \rho_c 4\pi R^3 / 3 = m$, with ρ_c the critical density of the universe.

In this limit, the halo-halo correlation function becomes $\xi_{hh}(r|m, m') = \bar{b}(m) \bar{b}(m') \xi_{\text{lin}}(r)$ and thus the cluster-cluster correlation function simplifies to:

$$\xi_{\vec{a},\vec{a}'}^t(r) = \bar{b}_{\vec{a}}^t \bar{b}_{\vec{a}'}^t \xi_{\text{lin}}(r)\tag{7}$$

where

$$\bar{b}_{\vec{a}}^t \equiv \int_0^\infty dm \frac{\bar{n}(m)}{\bar{n}_{\vec{a}}^t} \bar{b}(m) \bar{\psi}_{\vec{a}}(m).\tag{8}$$

Not surprisingly, we see that the cluster-cluster correlation function traces the underlying mass correlation function. It is worth pointing out that observationally the power spectra of galaxies and clusters are seen to have the same shape but different amplitude on scales $k^{-1} \sim 10$ Mpc or larger, so that the simple scale-independent linear bias is indeed feasible on large scales [48] (in fact, it is necessarily so for gaussian fields [44]).

III. INTRINSIC ERRORS ESTIMATE

We discuss now three intrinsic uncertainties associated with our observables: Poisson errors, sample variance, and uncertainties due to intrinsic scatter in the mass-tracer to mass scaling relation. Keeping an eye on our choice of model survey in §V, we assume a volume limited sample such that all objects of interest (i.e. all halos with η in the range of interest) are detected. Further, we assume no contamination of the sample, and a perfect instrument so that the observed value η^{obs} of the mass tracer always matches the true value η^{true} . Experimental bias and scatter are treated in §IV.

³ We have chosen to denote this quantity \bar{b} since the expression depends on the average halo mass function $\bar{n}(m)$ rather than $n(m, \vec{x})$.

A. Poisson Uncertainties and Sample Variance

The first type of uncertainty is the Poisson error in the number of clusters found. Assuming no intrinsic clustering, the variance in the density of clusters is simply given by \bar{n}_a^t/\bar{V} . This contribution to the correlation matrix is therefore

$$\tilde{C}_{\bar{a},\bar{a}'}^{nn}|_{Poisson} \equiv \langle (n_{\bar{a}} - \bar{n}_{\bar{a}}^t)(n_{\bar{a}'} - \bar{n}_{\bar{a}'}^t) \rangle^{Poisson} = \delta_{\bar{a},\bar{a}'} \frac{\bar{n}_{\bar{a}}^t}{\bar{V}}. \quad (9)$$

Note the use of the symbol $\tilde{C}_{\bar{a},\bar{a}'}$ for the correlation matrix. We include a \sim above the C to identify it as the “intrinsic” correlation matrix, meaning that no observational effects have been taken into account. There is also a Poisson term in the bias arising from the estimation of the clustering properties with a finite number of galaxies (namely the second term in equation 34) which is treated later on to properly account for contamination and completeness.

In addition to this, Hu and Kravtsov showed that sample variance becomes increasingly important as we probe lower and lower mass scales [22] in the halo mass function. We rederive here the result for sample variance found in Hu and Kravtsov, to use it as a reference for deriving the sample variance errors involving bias.

Assuming we have averaged over $P(\eta|m)$ (uncertainties associated with this probability are derived below), the sample variance contribution to the density-density correlation matrix is given by

$$\tilde{C}_{\bar{a},\bar{a}'}^{nn}|_{sample} = \int d^3x d^3x' W(\vec{x})W(\vec{x}') \int dmdm' \langle \psi_{\bar{a}}|m \rangle \langle \psi_{\bar{a}'}|m' \rangle \{ \langle n(m, \vec{x})n(m', \vec{x}') \rangle - \bar{n}(m)\bar{n}(m') \}$$

where $W(\vec{x})$ is the survey’s window function. Note we do not include terms proportional to simultaneous deviations from the mean due to sample variance and the variance of $\psi_{\bar{a}}$ due to $P(\eta|m)$ as these would yield only small corrections.

We approximate $W(\vec{x})$ above to be a spherical top-hat function encompassing a volume equal to that of the survey volume. The matrix element can now be easily computed by replacing $n(m, \vec{x})$ in the above expressions with $\bar{n}(m) + \delta n(m, \vec{x})$ where $\delta n = \bar{b}(m)\bar{n}(m)\delta$. Since $\langle \delta \rangle = 0$ and $\langle \delta \delta \rangle = \xi(\vec{x} - \vec{x}')$, we obtain then

$$\begin{aligned} \tilde{C}_{\bar{a},\bar{a}'}^{nn}|_{sample} &= \bar{n}_{\bar{a}}^t \bar{n}_{\bar{a}'}^t \bar{b}_{\bar{a}}^t \bar{b}_{\bar{a}'}^t \int d^3k P(k) |W(k)|^2 \\ &= \bar{n}_{\bar{a}}^t \bar{n}_{\bar{a}'}^t \bar{b}_{\bar{a}}^t \bar{b}_{\bar{a}'}^t \sigma^2(R_V). \end{aligned} \quad (10)$$

where R_V is given by $4\pi R_V^3/3 = V$. This is the final result that we were looking for, namely an expression for the covariance matrix between the number of objects found in each bin due to sample variance. The total density-density correlation matrix is obtained then by adding the sample variance matrix and the Poisson noise.

Let us now turn towards matrix elements involving bias. As before, the sample variance contribution is

$$\tilde{C}_{\bar{a},\bar{a}'}^{nb}|_{sample} = \int d^3x d^3x' W(\vec{x})W(\vec{x}') \int dmdm' \langle \psi_{\bar{a}}|m \rangle \langle \psi_{\bar{a}'}|m' \rangle \{ \langle n(m, \vec{x})b(m', \vec{x}') \rangle - \bar{n}(m)\bar{b}(m') \}$$

Again, we replace $n(m, \vec{x})$ by $\bar{n}(m) + \delta n(m, \vec{x})$ and $b(m, \vec{x}') by $\bar{b}(m) + \delta b(m, \vec{x}')$. To get an expression for δb , we generalize Eq. (6) to unbarred b and n , so that$

$$\bar{b} + \delta b = 1 - \frac{\partial}{\partial \delta_{sc}} (\ln(\bar{n}(1 + \bar{b}\delta))) \quad (11)$$

$$= \bar{b} - \delta \frac{\partial \bar{b}}{\partial \delta_{sc}} \quad (12)$$

where the second equality holds to leading order in δ . Hence

$$\delta b = -\delta \frac{\partial \bar{b}}{\partial \delta_{sc}}. \quad (13)$$

With this result, the sample variance contribution to $\tilde{C}_{\bar{a},\bar{a}'}^{nb}$ may be written as

$$\tilde{C}_{\bar{a},\bar{a}'}^{nb}|_{sample} = \bar{n}_{\bar{a}}^t \bar{b}_{\bar{a}}^t \bar{b}_{\bar{a}'}^t \bar{c}_{\bar{a}}^t \sigma^2(R_V) \quad (14)$$

where

$$\bar{c}_{\bar{a}}^t = \int dm \frac{\bar{n}(m)\bar{b}(m)}{\bar{n}_{\bar{a}}\bar{b}_{\bar{a}}} \bar{\psi}_{\bar{a}}(m) \left(-\frac{\partial \bar{b}}{\partial \delta_{sc}} \right) \quad (15)$$

In exactly the same way we obtain the bias-bias terms of the correlation matrix, which are given by

$$\tilde{C}_{\bar{a},\bar{a}'}^{bb}|_{sample} = \bar{b}_{\bar{a}}^t \bar{b}_{\bar{a}'}^t \bar{c}_{\bar{a}}^t \bar{c}_{\bar{a}'}^t \sigma^2(R_V). \quad (16)$$

B. Mass Tracer Dispersion Errors

By mass tracer dispersion errors we mean the uncertainties in the density and bias of objects in a given bin \vec{a} due to the fact that η is not uniquely determined by m , i.e. uncertainties due to the probability distribution $P(\eta|m)$. Note these are somewhat analogous to Poisson uncertainties in the number of galaxies in a spatial bin. Not surprisingly, then, the uncertainties take on a form $\delta n \sim n/\bar{V}$ where \bar{V} is the volume of the survey.

Consider then a realization of the halo model. Given the survey volume \bar{V} , the number density of objects in bin \vec{a} in one realization may be written as

$$n_{\vec{a}}^t = \frac{1}{\bar{V}} \sum_i \nu_i \psi_{\vec{a}}(\eta(m_i))$$

where ν_i is the number of halos in the mass bin m_i . The mass binning must be chosen small enough so that at most one halo is found in any given mass bin. This ensures η_i is a random variable for each halo (i.e. that η_i and η_j are uncorrelated for any two halos i, j). We have then

$$\begin{aligned} \overline{n_{\vec{a}}^t n_{\vec{a}'}^t} &= \frac{1}{\bar{V}^2} \sum_i \left\{ \sum_{j \neq i} \nu_i \nu_j \langle \psi_{\vec{a}}(\eta(m_i)) \psi_{\vec{a}'}(\eta(m_j)) \rangle + \nu_i^2 \langle \psi_{\vec{a}}(\eta(m_i)) \psi_{\vec{a}'}(\eta(m_i)) \rangle \right\} \\ &= \frac{1}{\bar{V}^2} \sum_i \left\{ \sum_{j \neq i} \nu_i \nu_j \langle \psi|m_i \rangle \langle \psi_{\vec{a}'}|m_j \rangle + \nu_i \langle \psi_{\vec{a}}(\eta(m_i)) \psi_{\vec{a}'}(\eta(m_i)) \rangle \right\} \end{aligned} \quad (17)$$

We have used above that $\eta(m_i)$ and $\eta(m_j)$ are not correlated, and that $\nu_i^2 = \nu_i$ (since $\nu_i = 0, 1$). We may write a similar expression for $\bar{n}_{\vec{a}}^t \bar{n}_{\vec{a}'}^t$,

$$\bar{n}_{\vec{a}}^t \bar{n}_{\vec{a}'}^t = \frac{1}{\bar{V}^2} \sum_i \left\{ \sum_{j \neq i} \nu_i \nu_j \langle \psi_{\vec{a}}|m_i \rangle \langle \psi_{\vec{a}'}|m_j \rangle + \nu_i \langle \psi_{\vec{a}}|m_i \rangle \langle \psi_{\vec{a}'}|m_i \rangle \right\} \quad (18)$$

so upon subtracting Eq. (18) from Eq. (17), we find

$$\tilde{C}_{\vec{a}, \vec{a}'}^{nn} |_{\text{mass tracer}} = \frac{1}{\bar{V}^2} \sum_i \nu_i C_{\vec{a}, \vec{a}'}^{\psi\psi}(m_i)$$

where

$$C_{\vec{a}, \vec{a}'}^{\psi\psi}(m) = \langle \psi_{\vec{a}}(\eta(m)) \psi_{\vec{a}'}(\eta(m)) \rangle - \langle \psi_{\vec{a}}|m \rangle \langle \psi_{\vec{a}'}|m \rangle \quad (19)$$

But note that ν_i/\bar{V} is just the average number density of halos in a bin of mass m_i . Averaging over many realizations, we have

$$\left\langle \frac{\nu_i}{\bar{V}} \right\rangle = \bar{n}(m_i) \Delta m_i$$

and hence

$$\tilde{C}_{\vec{a}, \vec{a}'}^{nn} |_{\text{mass tracer}} = \frac{1}{\bar{V}} \sum_i \Delta m_i \bar{n}(m_i) C_{\vec{a}, \vec{a}'}^{\psi\psi}(m_i).$$

In the continuum limit, we obtain our final answer,

$$\tilde{C}_{\vec{a}, \vec{a}'}^{nn} |_{\text{mass tracer}} = \frac{1}{\bar{V}} \int dm \bar{n}(m) C_{\vec{a}, \vec{a}'}^{\psi\psi}(m) \quad (20)$$

where $C_{\vec{a}, \vec{a}'}^{\psi\psi}$ is given by equation (19). If the binning function satisfies $\psi_{\vec{a}}(\eta) \psi_{\vec{a}'}(\eta) = \delta_{\vec{a}, \vec{a}'} \psi_{\vec{a}}(\eta)$ (e.g. non-overlapping top-hat bins) equation (19) simplifies to

$$C_{\vec{a}, \vec{a}'}^{\psi\psi}(m) = \delta_{\vec{a}, \vec{a}'} \langle \psi_{\vec{a}}|m \rangle - \langle \psi_{\vec{a}}|m \rangle \langle \psi_{\vec{a}'}|m \rangle. \quad (21)$$

Our expression for the contribution to the correlation matrix from $P(\eta|m)$ makes sense. If $P(\eta|m)$ is very narrow, then a given mass m will always get assigned to one and only bin \vec{a} . In that case, $\langle \psi_{\vec{a}}|m \rangle = 1$, and Eq. (21) shows

that the correlation matrix vanishes. That is, if the mass tracer is perfect, then there is no uncertainty associated with it. In the more realistic case, a mass m will sometimes be assigned to more than one bin. Then, the second term in Eq. (21) would be non-zero even if $\vec{a} \neq \vec{a}'$. This would lead then to an anti-correlation between these two bins. Because of the leakage into adjoining bins, $\langle \psi_{\vec{a}} | m \rangle < 1$ and the diagonal term in $C^{\psi\psi}$ also becomes nonzero.

What about density-bias terms? Going back to equation (8), we can write the bias as

$$b_{\vec{a}}^t = \frac{1}{\bar{n}_{\vec{a}}^t V} \sum_i \nu_i b(m_i) \psi_{\vec{a}}(\eta(m_i))$$

A procedure analogous to the one before yields

$$\tilde{C}_{\vec{a}, \vec{a}'}^{mb} = \frac{1}{\bar{n}_{\vec{a}'}^t V^2} \sum_i \nu_i b(m_i) C_{\vec{a}, \vec{a}'}^{\psi\psi}(m_i).$$

Converting this into an integral, we get

$$\tilde{C}_{\vec{a}, \vec{a}'}^{mb} = \frac{1}{\bar{n}_{\vec{a}}^t V} \int dm \bar{n}(m) \bar{b}(m) C_{\vec{a}, \vec{a}'}^{\psi\psi}(m) \quad (22)$$

Incidentally, note that the correlation matrix is still symmetric despite the appearance of a factor $1/\bar{n}_{\vec{a}'}^t$. The matrix element across the diagonal is $\tilde{C}_{\vec{a}', \vec{a}}^{bn}$, which also contains the same $1/\bar{n}_{\vec{a}'}^t$ factor. All other terms in the expression are clearly symmetric.

Finally, performing the same analysis yields the bias-bias contribution, given by

$$\tilde{C}_{\vec{a}, \vec{a}'}^{bb} = \frac{1}{V} \frac{1}{\bar{n}_{\vec{a}}^t \bar{n}_{\vec{a}'}^t} \int dm \bar{n}(m) \bar{b}(m)^2 C_{\vec{a}, \vec{a}'}^{\psi\psi}(m). \quad (23)$$

IV. OBSERVATION RELATED UNCERTAINTIES AND SYSTEMATICS

We have derived above expressions for the density and bias of halos binned according to an unspecified mass tracer η , along with the related intrinsic uncertainties assuming a volume limited survey. We have, however, been assuming no contamination, 100% rate detection (completeness), and the ability to observe η precisely. We wish to incorporate into our formalism uncertainties and systematic effects arising from observation. In particular, we assume observational effects may be characterized by the following information:

- The average detection rate (completeness) $\bar{r}_{\vec{a}}$ and its variance $C_{\vec{a}, \vec{a}'}^{rr}$. $\bar{r}_{\vec{a}}$ is defined as the fraction of objects in bin \vec{a} which are identified.
- The average false detection rate $\bar{f}_{\vec{a}}$ and its variance $C_{\vec{a}, \vec{a}'}^{ff}$. $\bar{f}_{\vec{a}}$ is defined as the number of spurious objects per unit volume in bin \vec{a} .
- The probability $q(\eta|\eta^t)$ that a halo with observed η has a true value η^t .

Note we made the simplifying assumption that both $r_{\vec{a}}$ and $f_{\vec{a}}$ are position independent, though it is straightforward (albeit cumbersome) to extend the formalism to include position dependent detection and contamination rates.

We begin by incorporating detection and contamination rates into the formalism. Further, since the true observable is not the density of objects but rather the number of objects in a given bin, we modify our formalism appropriately. Given our assumptions, the number of objects identified in a volume limited survey takes the form

$$N_{\vec{a}} = (r_{\vec{a}} n_{\vec{a}}^t + f_{\vec{a}}) V \quad (24)$$

where $n_{\vec{a}}^t$ is the average number of objects in bin \vec{a} . The corresponding correlation matrix is then⁴

$$C_{\vec{a}, \vec{a}'}^{NN} = C_{\vec{a}, \vec{a}'}^{rr} \bar{n}_{\vec{a}}^t \bar{n}_{\vec{a}'}^t \bar{V}^2 + \bar{r}_{\vec{a}} \bar{r}_{\vec{a}'} \bar{V}^2 \tilde{C}_{\vec{a}, \vec{a}'}^{nn} + C_{\vec{a}, \vec{a}'}^{ff} \bar{V}^2 + \frac{\bar{N}_{\vec{a}}}{\bar{V}} \frac{\bar{N}_{\vec{a}'}}{\bar{V}} (\Delta V)^2$$

⁴ Throughout, we are using the fact that

$$\alpha_i = a_i b_i + c_i \Rightarrow C_{ij}^{\alpha\alpha} = \bar{a}_i \bar{a}_j C_{ij}^{bb} + \bar{b}_i \bar{b}_j C_{ij}^{aa} + C_{ij}^{cc}.$$

Terms involving products of correlation matrices are being ignored as second order terms. For the expression above, a_i , b_i , and c_i are all uncorrelated with each other and possess different probability distributions (which is the case of interest here).

$$= \frac{\bar{N}_{\vec{a}} - \bar{f}_{\vec{a}}\bar{V}}{\bar{r}_{\vec{a}}} \frac{\bar{N}_{\vec{a}'} - \bar{f}_{\vec{a}'}\bar{V}}{\bar{r}_{\vec{a}'}} C_{\vec{a},\vec{a}'}^{rr} + \bar{V}^2 C_{\vec{a},\vec{a}'}^{ff} + \bar{r}_{\vec{a}}\bar{r}_{\vec{a}'}\bar{V}^2 \tilde{C}_{\vec{a},\vec{a}'}^{nn} + \bar{N}_{\vec{a}}\bar{N}_{\vec{a}'} \frac{(\Delta V)^2}{\bar{V}^2} \quad (25)$$

where $(\Delta V)^2$ is the variance in the volume arising from uncertainties in the measured redshifts of the clusters. The result is just what one would expect: the uncertainties for a perfect algorithm $\tilde{C}_{\vec{a},\vec{a}'}^{nn}$ are scaled by the detection factors. In addition, one adds the uncertainties due to imperfect knowledge of the detection and false detection rates. Finally one needs to include the contribution from uncertainties in the sampled volume arising from redshift uncertainties. The expression above simplifies when the detection and contamination rates of different bins are uncorrelated, in which case one obtains

$$C_{\vec{a},\vec{a}'}^{NN} = \delta_{\vec{a},\vec{a}'} \left\{ (\bar{N}_{\vec{a}} - \bar{f}_{\vec{a}}\bar{V})^2 \frac{(\Delta r_{\vec{a}})^2}{\bar{r}_{\vec{a}}^2} + (\bar{V}\Delta f_{\vec{a}})^2 \right\} + \bar{r}_{\vec{a}}\bar{r}_{\vec{a}'}\bar{V}^2 \tilde{C}_{\vec{a},\vec{a}'}^{nn} + \bar{N}_{\vec{a}}\bar{N}_{\vec{a}'} \frac{(\Delta V)^2}{\bar{V}^2}. \quad (26)$$

We wish to incorporate now systematic effects and/or uncertainties in the assigned cluster richness arising from the observations. In particular, we wish to include the fact that binning of data is done in terms of the *observed* value of η rather than the true value η^t . We view the observations as providing a random mapping $\eta(\eta^t)$ where a value η has a probability $q(\eta|\eta^t)$ of occurring. The probability $q(\eta|\eta^t)$ is assumed to be known from experimental calibrations. e.g. if we consider X-ray temperature measurements for a cluster, $q(T|T^t)$ describes how a series of measurements T_i of a cluster with temperature T^t is distributed.

Consider then the number of objects in a bin \vec{a} . All we need to do then is replace $\psi_{\vec{a}}(\eta^t)$ by $\psi(\eta)$ where η is the observed value. The relevant probability for computing $\bar{\psi}_{\vec{a}}(m) = \langle \psi_{\vec{a}}(\eta)|m \rangle$ is not $P(\eta^t|m)$ but $\tilde{P}(\eta|m)$, the probability of observing a value η given a halo mass m . This is given by

$$\tilde{P}(\eta|m) = \sum_{\eta^t} q(\eta|\eta^t) P(\eta^t|m). \quad (27)$$

By replacing η by η^t and $P(\eta^t|m)$ by $\tilde{P}(\eta|m)$ in formulae, we obtain expressions for the number density and bias of halos binned according to the observed value η . Any systematic effects and/or uncertainties introduced by the observations will automatically be taken into account in the convolution of $q(\eta|\eta^t)$ and $P(\eta^t|m)$. Note though that an application of our formalism requires an understanding of the probability $q(\eta|\eta^t)$, presumably characterized in the experiment's calibration.

Let us now turn our attention to bias. The density of detected groups in bin \vec{a} , which we shall denote $n_{\vec{a}}$ (note the superscript t is missing), is given by

$$n_{\vec{a}}(\vec{x}) = r_{\vec{a}} n_{\vec{a}}^t(\vec{x}) + f_{\vec{a}}$$

where we are assuming a detection rate $r_{\vec{a}}$ and a false detection rate $f_{\vec{a}}$, known from calibration to have values $\bar{r}_{\vec{a}}$ and $\bar{f}_{\vec{a}}$ and variances $C_{\vec{a},\vec{a}'}^{rr}$ and $C_{\vec{a},\vec{a}'}^{ff}$.⁵ With these assumptions, the observed correlation function is given by

$$\bar{n}_{\vec{a}}\bar{n}_{\vec{a}'}\xi_{\vec{a},\vec{a}'}^{nn} = \bar{r}_{\vec{a}}\bar{r}_{\vec{a}'}\bar{n}_{\vec{a}}^t\bar{n}_{\vec{a}'}^t\xi_{\vec{a},\vec{a}'}^{t,nn}. \quad (28)$$

Replacing $\xi_{\vec{a},\vec{a}'}^{t,nn} = b_{\vec{a}}^t b_{\vec{a}'}^t \xi_{\text{lin}}$, and dividing through by $\bar{n}_{\vec{a}}\bar{n}_{\vec{a}'}$ we obtain

$$\xi_{\vec{a},\vec{a}'}^{nn} = b_{\vec{a}} b_{\vec{a}'} \xi_{\text{lin}} \quad (29)$$

where

$$\begin{aligned} b_{\vec{a}} &= \frac{\bar{n}_{\vec{a}}^t \bar{V}}{\bar{N}_{\vec{a}}} \bar{r}_{\vec{a}} b_{\vec{a}}^t \\ &= \left(\frac{\bar{N}_{\vec{a}} - \bar{f}_{\vec{a}} \bar{V}}{\bar{N}_{\vec{a}}} \right) b_{\vec{a}}^t. \end{aligned} \quad (30)$$

⁵ Note we are making use of our simplifying assumption that $r_{\vec{a}}$ and $f_{\vec{a}}$ do not depend on position. Otherwise, there would be systematic corrections to equation (28) due to the correlation functions of $r_{\vec{a}}$ and $f_{\vec{a}}$. These effects are easily incorporated, but we choose not to in the spirit of simplicity.

The expectation value of the observed bias is therefore simply

$$\bar{b}_{\bar{a}} = \left(\frac{\bar{N}_{\bar{a}} - \bar{f}_{\bar{a}} \bar{V}}{\bar{N}_{\bar{a}}} \right) \bar{b}_{\bar{a}}^t. \quad (31)$$

The observed bias is thus expected to be lower than the true bias due to the dilution of true clusters with false detections. The clustering signal, however, does not depend on $r_{\bar{a}}$. This is not surprising, as $r_{\bar{a}}$ changes only how many clusters we observe, but not their clustering properties. Of course, a lower $r_{\bar{a}}$ will lead to more noisy estimations of the bias (see equation 34).

Now that we have our expression for bias, we may compute the corresponding uncertainties. Using equations (24) and (30), we obtain

$$C_{\bar{a}, \bar{a}'}^{Nb} = \left(\frac{\bar{N}_{\bar{a}'} - \bar{f}_{\bar{a}'} \bar{V}}{\bar{N}_{\bar{a}'}} \right) (\bar{r}_{\bar{a}} \bar{V} \tilde{C}_{\bar{a}, \bar{a}'}^{nb}). \quad (32)$$

We can understand the expression above qualitatively. The factor $\bar{r}_{\bar{a}} \bar{V}$ in front of $\tilde{C}_{\bar{a}, \bar{a}'}^{nb}$ scales the correlation matrix to the total number of real clusters as opposed to number density. The prefactor corresponds to the scaling from the true bias to the observed bias.

Finally, this same type of analysis gives us the bias-bias terms of the observable's correlation matrix, resulting in

$$C_{\bar{a}, \bar{a}'}^{bb} = \left(\frac{\bar{N}_{\bar{a}} - \bar{f}_{\bar{a}} \bar{V}}{\bar{N}_{\bar{a}}} \right) \left(\frac{\bar{N}_{\bar{a}'} - \bar{f}_{\bar{a}'} \bar{V}}{\bar{N}_{\bar{a}'}} \right) \tilde{C}_{\bar{a}, \bar{a}'}^{bb}. \quad (33)$$

In addition to the errors above, there is a contribution coming from actually attempting to estimate bias from data. For instance, assuming the bias is measured using the power spectrum involves Fourier space discretization. This, in turn, brings its own set of sample variance errors, as well as Poisson errors in the number of objects found in a Fourier pixel. The corresponding errors in the power spectrum estimation are given by (see e.g. [7, 16, 49]):

$$\left(\frac{\Delta b_{\bar{a}}(k)}{b_{\bar{a}}} \right)^2 \approx \frac{2}{V V_k} \left(1 + \frac{1}{\bar{n}_{\bar{a}}(\bar{b}_{\bar{a}})^2 P(k)} \right) \quad (34)$$

where V is the volume of the survey, and V_k is the volume of the corresponding k -shell in Fourier space. i.e. $V_k \approx 4\pi k^2 \Delta k$ where Δk is the minimum spacing between k modes. Note the error estimate above $\Delta b_{\bar{a}}(k)$ depends on the wavenumber k used to estimate $b_{\bar{a}}$. One may average the estimated $b(k)$ over a large k range to obtain smaller errors. This diagonal contribution to the bias-bias correlation matrix must be added to that in equation (16) since it represents uncertainties in the experimental estimation of the bias parameter.

V. APPLICATION: GROUP AND CLUSTER STATISTICS IN A VOLUME LIMITED GALAXY SURVEY

We now apply our formalism to a hypothetical cluster catalogue obtained from a large volume limited galaxy survey. We are interested in particular in what kind of information we can extract from such a catalogue. We present below our assumptions as to how the hypothetical catalogue is built, followed by how the halo model formalism is applied in this particular case. We also present the fiducial model used in the next section to derive the type of constraints one can expect for these type of surveys.

A. Assumptions on the Cluster Catalogue

Given a galaxy sample, one may attempt to identify groups and clusters of galaxies within it. While the notions of clusters and cluster richness are intuitive, ultimately one needs precise definitions to obtain a well defined sample. This task is achieved via automated cluster finding algorithms. At present, there exist a large number of said algorithms, e.g. maxBCG [2], Hybrid Match Filter (HMF) [28], Cut and Enhance method (CE) [20], Vornoi Tessellation Technique (VTT) [28], C4 algorithm ([38],[37]), and Friends-of-Friends (FoF) [23], all of which simultaneously identify clusters (based on a specific set of criteria) and assign a richness measure to the identified clusters. The richness measures are typically the number of galaxies assigned to the cluster, or some measure of the cluster's total optical luminosity. If we identify clusters with massive halos, the richness measure provides then an observable which serves as a mass indicator. We can thus use our formalism to describe statistical properties of cluster catalogues by using the richness as the mass tracer η .

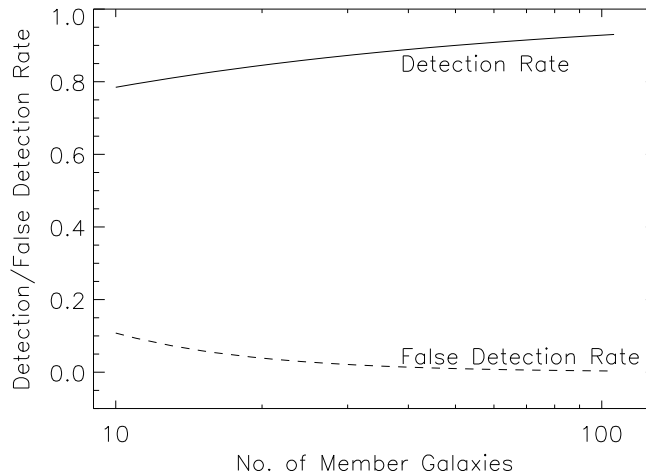


FIG. 1: The assumed detection and false detection rates are shown here with the solid and dashed line respectively. Note the latter is defined here in terms of the percentage of identified cluster that are false detections.

In this paper, we assume a cluster finding algorithm having a specified set of criteria to determine when a galaxy belongs (is assigned to) a cluster. The number of galaxies N assigned to a cluster will be our richness measure. Examples of this type of algorithm are maxBCG, C4, Friends-of-Friends, Voronoi Tessellation Technique⁶, and the cut and enhance method. For our hypothetical catalogue, we will not worry about what the exact criteria for cluster membership is for a galaxy: we simply need to assume such a criteria exists.⁷

Within this framework, then, the mass tracer is the number of galaxies in a halo N^t while the observed richness measure is N , the number of galaxies assigned to a cluster by the cluster finding algorithm. $q(N|N^t)$ is the probability that the cluster finding algorithm will assign N galaxies to a halo containing N^t galaxies. Likewise, \bar{r}_a and \bar{f}_a are the detection and false identification rates for the cluster finding algorithm.⁸

We make the further assumption that \bar{r}_a and \bar{f}_a are uncorrelated between various bins and with each other.

It is worth pointing out that at least some cluster finding algorithms (e.g. match filter algorithms) have a detection rate that is dependent on the galaxy background (see e.g. Kim et al. [28]). We will ignore this effect here. To include it, one could imagine the detection rate having the form $r_a = \bar{r}_a(1 + \gamma\delta_g)$ where δ_g is the galaxy density contrast and γ is a constant. Notice γ is a measure of whether r_a is strongly dependent on the background density or not. Using $\delta_g \approx \delta$ (since galaxies are unbiased tracers of mass), we could replace the above expression in equation 22 and rederive the corresponding uncertainties as in the previous section. This would add terms proportional to γ , which may be neglected in the limit that γ goes to zero. We do not expect this effect to have major consequences in our results.

Let us then specify the characteristics of our hypothetical cluster finding algorithm. We will assume that the non-detection rate (i.e. $1 - \bar{r}_a$), the false detection rates, and their errors, are all power laws as a function of the number of galaxies in the cluster. Thus, e.g., the detection rate is taken to have the form

$$\bar{r}_N = 1 - (N/N_0)^{-\gamma} \quad (35)$$

where N_0 and γ are constants. The normalization is specified by indicating their corresponding values for clusters with 5 galaxies and clusters with 50 galaxies, shown below, as well as the corresponding values N_0 and γ . Figure 1 plots the corresponding rates.

⁶ The Voronoi Tessellation Technique as given in Kim et al. [28] assigns richness using the match filter method. Nevertheless, one could imagine using the number of galaxies N that the VTT technique assigns to the cluster as a richness measure.

⁷ We note though that the membership criterion will in general affect the expected mass-richness relation, e.g. the number of member galaxies will clearly depend on the radius used to determine membership.

⁸ Note we are not considering q to give rise to false detections or imperfect detection rates. If a cluster is identified, but its richness is mislabelled, that effect is encoded in $q(N|N^t)$. On the other hand, a cluster that is broken up into two smaller clusters, or merged with another cluster to produce a larger one cannot be considered as a mislabelled cluster. In particular, these last two effects would greatly alter the richness and ruin the one-to-one and onto nature of the mapping between N and N^t that we have been assuming. The inclusion of detection rates and false detections here serves to naively account for these effects.

Rate/Error	N=5	N=50	N ₀	γ
\bar{r}_N	70%	90%	0.400	0.477
$\Delta\bar{r}_N$	10%	1%	0.500	1.000
\bar{f}_N	30%	1%	2.213	1.477
$\Delta\bar{f}_N$	10%	1%	0.500	1.000

Note that the false detection rate corresponds to the percentage of detected clusters in the fiducial model which are false detections. Thus, e.g. we are assuming that 30% of all detected clusters with 5 member galaxies are false detections. The correct values for the different type of algorithms vary, but we believe that the numbers above should provide a fair picture of the capabilities of cluster finding algorithms at low redshifts. Details on particular algorithms may be found in the references (see e.g. [2], [28], [20], [28], [38], [37], [23]).

Also note that when we apply our formalism we will need to assume that the data is binned into various richness classes, i.e. into bins of clusters containing N galaxies where $N_{max} > N \geq N_{min}$. We will use the same detection rate for all objects in a given bin, the detection rate being defined as the average rates for clusters with richness N_{min} and N_{max} .

Finally, we need to specify the probability that the algorithm assigns N galaxies to a cluster given that its parent halo has N^t galaxies (i.e. what we had called $q(\eta|\eta^t)$ earlier). It is difficult to find within the literature expressions for this probability. Here, we assume that the number of galaxies assigned to a halo takes the form $N = N^t + \delta N$ where δN is a random variable with an exponential distribution.⁹ In other words, we take $q(N|N^t) = P(\delta N)$ with P given by

$$P(\delta N|N^t) = A \exp(-a(N^t)|\delta N|). \quad (36)$$

The parameters A, a in the above expression are determined by the condition that the probabilities add to one, and by requiring that the expectation value of $|\delta N|$ be 10% of N^t .¹⁰ Note this distribution is wider than a Gaussian.

It is often the case that cluster finding algorithms systematically underestimate the number of galaxies of a cluster. This effect is easily accommodated by correcting our expression for N to $N = f(N^t) + \delta N$ where $f(N^t)$ is the average number of galaxies assigned to clusters with N^t galaxies. Since the only effect this brings about is a rescaling of the axis, we do not expect our conclusions to be changed due to possible biases in the galaxy assignments of cluster finding algorithms (provided, of course, that they are appropriately calibrated).

As a closing note, we would like to emphasize that all results presented here depend on the ability to accurately calibrate cluster finding algorithms. In particular, recall the parameter $a(N^t)$ in equation 36 is determined by demanding the expectation value of $|\delta N|$ to satisfy $\langle |\delta N| \rangle = cN^t$ where the value $c = 10\%$ was arbitrarily chosen. In general, marginalization over the c parameter as determined from calibrations will also be necessary, leading to a degradation of the confidence regions presented here.

B. The Halo Occupation Distribution

In order to apply our formalism, we need an expression for $P(N^t|m)$, the probability for a halo of mass m to have N^t galaxies in it. This probability is known as the Halo Occupation Distribution, or HOD. In accordance with the results of Kravtsov et al. [31], we assume all halos have a central galaxy, while any other galaxies found in the halo (referred to as satellite galaxies) are Poisson distributed with an average number

$$\langle N_{sat}|m \rangle = (m/M_1)^\alpha. \quad (37)$$

Here M_1 is the normalization parameter. It represents the mass of halos at which one expects, on average, to find 1 satellite galaxy. Prior galaxy formation simulations in which the distinction between host and satellite galaxies was not made agree with the results from Kravtsov et al. in that the number of galaxies in halos with large occupancy numbers is Poisson distributed with the average number increasing as a power law [9]. Furthermore, the power law assumption for $\langle N|m \rangle$ has been used to model the galaxy correlation function for both the 2dF survey and the SDSS survey with very good agreement (see e.g. Magliocchetti and Porciani [33] for the 2dF and Zehavi et al. [56] for the SDSS.) One may also wonder whether there is evidence that the probability $P(N^t)$ of a halo does depend indeed exclusively on the mass. Once again, simulations seem to indicate that this is indeed the case [9].

⁹ There is no reason to choose the distribution we used other than it is simple. We expect, however, that this distribution is at least qualitatively correct.

¹⁰ Again, the average value of $|\delta N|$ is arbitrarily chosen but we expect it to be representative.

C. Fiducial Model

1. Cosmology

The cosmological parameters used in our fiducial model are:

$$\begin{aligned}\Omega_m &= 0.3, \Omega_\Lambda = 0.7, \Omega_b h^2 = 0.049 \\ \sigma_8 &= 0.85, h = 0.7, n = 1.\end{aligned}$$

Here, n is the slope of the primordial power spectrum, which is filtered by the transfer function formulae from Hu and Eisenstein [21].

We also need to specify the halo mass function $\bar{n}(m)$ for the chosen cosmology. There are different prescriptions for obtaining $\bar{n}(m)$, the most well known being that of Press and Schechter [41]. Two other and more accurate mass functions are widely used in the literature, namely that of Sheth and Tormen [43], and that of Jenkins [26]. We use the Sheth-Tormen halo mass function since it can be physically motivated using elliptical collapse. The Sheth-Tormen halo mass function is given by:

$$\bar{n}(m) = \frac{\Omega_m \rho_c}{m} f(\nu) \frac{d\nu}{dm} \quad (38)$$

where

$$f(\nu) = A(1 + (q\nu)^{-p}) \left(\frac{q}{2\pi\nu}\right)^{\frac{1}{2}} \exp\left(-\frac{q\nu}{2}\right). \quad (39)$$

The value $A = 0.3222$ is obtained from numerical fits to N -body simulations, and recall from §II that $p = 0.3$, $q = 0.75$, and $\nu \equiv \delta_{sc}^2/\sigma^2(m)$.

2. HOD

We choose a halo occupation distribution in accord with our previous discussion, i.e. a host galaxy plus Poisson distributed satellite galaxies for all halos. The average number of satellite galaxies is given by equation (37) with

$$M_1 = 6.0 \times 10^{12} M_\odot \quad \alpha = 1.0.$$

The choice of the HOD parameters requires a little discussion. Both of the HOD parameters α and M_1 for large halo masses have been obtained empirically by doing halo model fits to the galaxy-galaxy correlation function as measured by the SDSS (see Zehavi et al. [56]) and the 2dF survey (see Magliocchetti and Porciani [33]). Zehavi et al. find a slope of $\alpha \approx 0.89$, while Magliocchetti and Porciani find $\alpha \approx 0.9$ for old galaxies, and $\alpha \approx 0.6$ for star forming galaxies (see [33] for details). Finally, Berlind et al. [9] find $\alpha \approx 0.9$ on the basis of numerical simulations. In all of these fits, however, no distinction between a central galaxy and satellite galaxies was made in any of these studies. Kravtsov et al. showed that in their N -body simulations this distinction gives better fits in N -body simulations, while raising the slope from 0.9 to 1.0 [31]. We have therefore opted to use a slope of 1 as the fiducial model in accord with dark matter simulations.¹¹ Note that there is evidence that the slope varies with galaxy type (early vs. late, [33]), so clearly the correct value of the slope will depend on the exact sample of galaxies we are looking at.

The mass parameter M_1 likewise depends on the particular galaxy sample under consideration. Most importantly, it depends critically on the intrinsic luminosity cutoff of the sample. For galaxies with intrinsic luminosity $M_r < -21$, Zehavi et al. find the value $M_1 \approx 1.0 \cdot 10^{14} M_\odot$.¹² The magnitude limit above corresponds to a galaxy density $\approx 10^{-3} h^3 \text{ gal/Mpc}^3$. Kravtsov et al. find a similar value for M_1 at said density. For a density $n = 2.79 \cdot 10^{-2} h^3 \text{ Mpc}^{-3}$, corresponding to galaxies brighter than $M_r \approx -18$ (Blanton et al. [10]), Kravtsov et al obtain $M_1 = 5 \cdot 10^{12} M_\odot$ [31]. Using semi-analytical and SPH simulations, Berlind et al [9] find $M_1 \approx 7 \cdot 10^{12} M_\odot$ for a comparable galaxy density.¹³ We assume here a value $M_1 = 6 \cdot 10^{12} M_\odot$ for the fiducial model.

¹¹ We note here that baryon cooling may lower the value of α . For instance, in massive halos, the cooling time may approach the hubble time, which may reduce galaxy formation efficiency. However, since we are not aware of either observational or galaxy formation simulation constraints on the halo occupation distribution where a distinction between host and satellite galaxies is made, we have opted to keep the value of α obtained from dark matter simulations.

¹² The value M_1 they quote is lower, but we have corrected it to take into account the assumption of a central galaxy. Zehavi quotes that at a mass of $\approx 4.5 \cdot 10^{14} M_\odot$, one expects 5.4 galaxies, corresponding to 4.4 satellite galaxies, or $M_1 \approx 1.0 \cdot 10^{14} M_\odot$ if $\alpha = 1$.

¹³ Note what we are calling M_1 here corresponds to M_{crit} in the Berlind et al. paper, i.e. the amplitude of $\langle N|m \rangle$ at high masses.

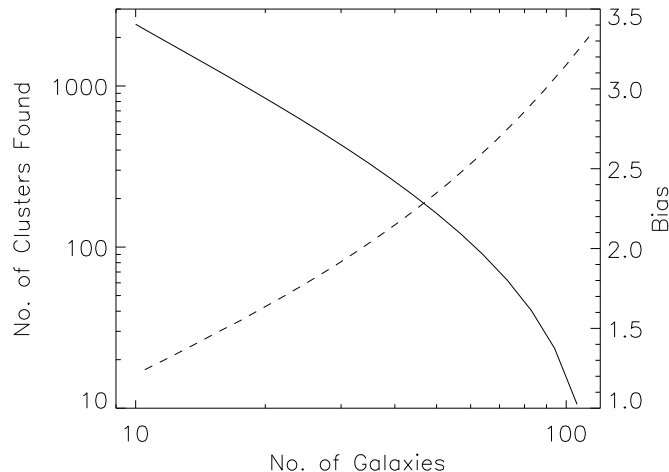


FIG. 2: We show above the predicted richness (solid line) and observed bias as a function of richness (dashed line) for our survey given our fiducial model. The richness function is defined as the number of clusters found having more than the specified minimum number of galaxies.

D. Survey Assumptions

We assume a 10^4 deg^2 sky survey which is the target SDSS coverage [55], and a volume limit of $z \leq 0.1$. In the fiducial cosmology, this corresponds to a volume of about $6 \cdot 10^7 \text{ Mpc}^3$. At our volume limit of $z = 0.1$, and for the SDSS telescope, one expects all galaxies with intrinsic magnitude $M \sim -18$ to be detected and have their redshift measured¹⁴ justifying our choice for M_1 in the fiducial model. Notice that while the volume V has some error ΔV arising from the fact that redshifts have some intrinsic error, we have set this term to zero assuming spectroscopic redshift of the galaxies is available. This is reasonable given our very shallow survey, though the error ΔV will become non-negligible in higher redshift surveys.

Finally, we assume all clusters in the catalogue are binned logarithmically into 20 different bins. We have checked this binning is fine enough to accurately contain all the information in our survey. The lowest and highest richness classes we consider are clusters with 10 and 120 galaxies respectively, which corresponds to a mass range between $M_{min} \sim 5 \cdot 10^{13} M_\odot$ and $M_{max} \sim 7 \cdot 10^{14} M_\odot$. The predicted cluster richness function is shown in figure 2.

One final note: we are considering bias to be our observable. To obtain the bias, one needs to fit the correlation function as a whole as $\xi = b^2 \xi_{LIN}$ (note ξ_{LIN} varies with cosmology). The fit gives the bias measurement, while the shape information is discarded. We expect then that the confidence regions we obtain here may be improved upon when the full information of the correlation function is used.

VI. RESULTS

A. Determination of the Confidence Regions

Now that we have the correlation matrix of our observables, we estimate the Fisher matrix for the HOD and cosmological parameters as (see e.g. [16])

$$F_{ab} = \sum_{ij} (C^{-1})_{ij} \frac{\partial O_i}{\partial \lambda_a} \frac{\partial O_j}{\partial \lambda_b} \quad (40)$$

where λ_a stands for the various parameters of interest and O_i label our various observables. As explained in [16], the matrix F serves as an approximation of the inverse correlation matrix for the parameters λ_a , which we use to compute

¹⁴ See <http://www.sdss.org/documents/goals.html>.

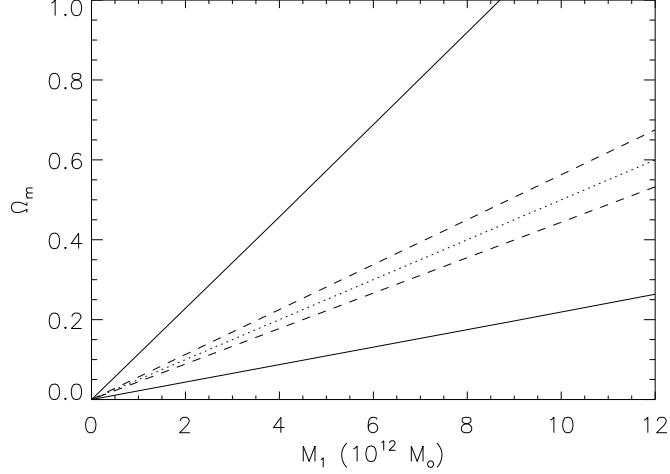


FIG. 3: The solid lines in this figure delimit the 95% confidence region marginalized over all parameters. Even moderately strong priors of $\Delta\alpha = 5\%$ and $\Delta\sigma_8 = 0.1$ do not improve the constraints much, though holding them fixed collapses the confidence region to that enclosed by the dashed lines. Finally, the dotted line corresponds to the contour $M_1/\Omega_m = \text{constant}$, the constant being set by the fiducial model. The 95% confidence limits on $\Omega_m M_1^{-1}$ are $\Omega_m M_1^{-1} = 5.0^{+4.8}_{-2.5} \cdot 10^{-14} M_\odot^{-1}$ (marginalized over α, σ_8) and $\Omega_m M_1^{-1} = 5.00^{+0.52}_{-0.47} \cdot 10^{-14} M_\odot^{-1}$ (α, σ_8 fixed).

the confidence regions reported here. Our observables in this case are the number of clusters found in each bin and their bias, and the parameters of interest are those specifying the cosmology and the HOD. The one caveat is that, to obtain the confidence regions, we will use as our parameters not the model parameters themselves (i.e. $\alpha, M_1, \sigma_8, \dots$) but their logarithms. There are two motivations behind this:

- Using the natural logarithms enforces positivity in all parameters.
- Traditionally, cluster surveys have been used to obtain constraints of the form $\sigma_8 \Omega_m^\gamma = \text{constant}$. These type of constraints are obtained as eigenvectors of the fisher matrix when the natural logarithm of the parameters of interest are used in computing the fisher matrix, so using logarithms should make comparison to previous work more straightforward.

Unless stated otherwise, all of our confidence regions and intervals will be marginalized over h, n , and $\Omega_b h^2$ using gaussian priors

$$\sigma_h = 0.1 \quad \sigma_n = 0.1 \quad \sigma_{\Omega_b h^2} = 0.002.$$

B. $M_1 - \Omega_m$ Degeneracy

The first thing we notice upon computation of the Fisher matrix is the existence of an extremely large degeneracy between M_1 and Ω_m of the form $\Omega_m/M_1 = \text{constant}$. This is shown graphically in figure 3. Here, we plot the 95% confidence region in the $\Omega_m - M_1$ plane when marginalizing over α and σ_8 (solid lines) and when holding them constant (dashed lines). The dotted line corresponds to the equation $\Omega_m/M_1 = \text{constant}$, the constant being set by the fiducial model. The 95% confidence constraint marginalized over all other parameters is $\Omega_m/M_1 = (5.0^{+4.8}_{-2.5}) \cdot 10^{-14} M_\odot^{-1}$, a rather poor constraint. The perpendicular direction $\Omega_m M_1 = \text{constant}$ is not constrained at all.

The reason for this degeneracy can be traced to the behavior of the mass function with Ω_m and the fact that our observable (number of galaxies in a cluster) scales as m/M_1 . To see this mathematically, first note that for the halo mass function of Eq. 38,

$$dm \bar{n}(m, \Omega_m) \approx dx F(x) \quad (41)$$

for $x = m/\Omega_m$ and F being some function. Equation 41 can be verified by referring back to equation 38. We see there that $\bar{n}(m, \Omega_m)$ takes the form

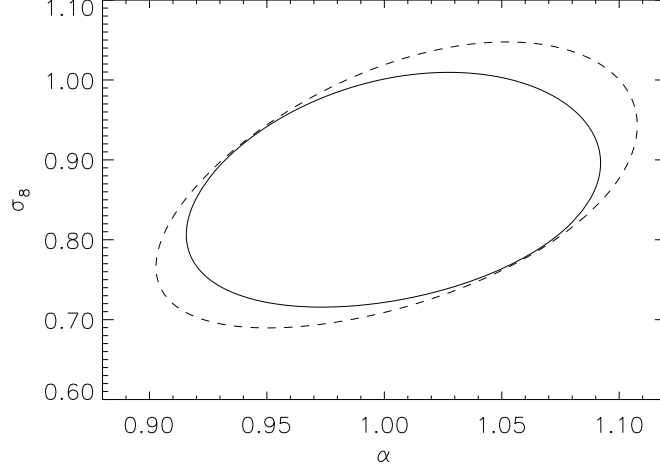


FIG. 4: The 95% confidence regions marginalized over the Hubble rate, spectral index, and baryon density using moderate gaussian priors. The outer dashed ellipse is also marginalized over M_1 and Ω_m without assuming any priors for these quantities. The inner solid ellipse is obtained assuming gaussian priors $\Omega_m = 0.3 \pm 0.1$ and $\Delta M_1/M_1 = 30\%$. The corresponding 95% confidence intervals are $\alpha = 1.000^{+0.085}_{-0.079}$ and $\sigma_8 = 0.85^{+0.16}_{-0.13}$, and $\alpha = 1.000^{+0.073}_{-0.068}$ and $\sigma_8 = 0.85^{+0.13}_{-0.11}$.

$$dm\bar{n} = (\Omega_m dx) \frac{\rho_c}{x} \frac{d\nu}{dm} f(\nu) \quad (42)$$

$$= dx \frac{\rho_c}{x} \frac{d\nu}{dx} f(\nu). \quad (43)$$

where $\nu = \delta_s c^2 / \sigma(R(m))^2$. Since $R(m)$ is given by the condition $4\pi R(m)^3 \Omega_m \rho_c = 3m$, it is clear that $R(m)$ depends only on x . Thus, if the power spectrum were independent of Ω_m , $\sigma(R(m))$, and hence \bar{n} , would depend only on x . There is then a small dependence of $\sigma(R(m))$ on Ω_m alone which comes through the power spectrum used in the convolution. This small dependence makes equation 41 only approximate.

Now, for a given mass m , the number of galaxies in the halo – and therefore the value of $\langle \psi_{\bar{a}} | m \rangle$ – depends via Eq. 37 only on (m/M_1) . That is, $\langle \psi_{\bar{a}} | m \rangle(m) = g(m/M_1)$ for some function g , so

$$\begin{aligned} \bar{n}_{\bar{a}} &= \int dm \bar{n}(m, \Omega_m) g(m/M_1) \\ &\approx \int dx F(x) g(\Omega_m x / M_1) \\ &= \phi(\Omega_m / M_1) \end{aligned} \quad (44)$$

where ϕ is a function. We see then that $\bar{n}_{\bar{a}}$ depends only the ratio M_1/Ω_m , so there is indeed a full degeneracy between the two parameters. Since the argument assumes only that the mass tracer scales as a function of m/M_1 where M_1 is a characteristic mass scale, we expect this degeneracy to be quite general. It is also easy to check that a similar computation holds for bias.

C. Constraints on α and σ_8

Despite the strong degeneracy between M_1 and Ω_m , it is still possible to constrain α and σ_8 without the use of any further priors. Shown in figure 4 with the dashed line is the 95% confidence region of the $\alpha - \sigma_8$ plane marginalized over Ω_m and M_1 assuming no priors for either of these two quantities. The constraints improve only slightly when invoking priors on either Ω_m or M_1 . Finally, the solid contour encloses the 95% confidence region with reasonable priors $\Delta\Omega_m = 0.1$ and $\Delta M_1/M_1 = 30\%$.

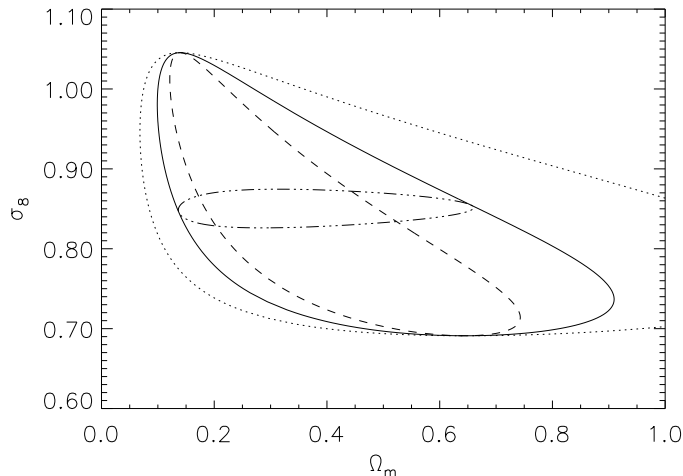


FIG. 5: The 95% confidence regions above are marginalized over the hubble rate, spectral index, and baryon density using moderate gaussian priors. In addition, we have assumed a gaussian prior for the M_1 parameter of width $\Delta M_1 = 50\%$ (dotted line), $\Delta M_1 = 30\%$ (solid line), and $\Delta M_1 = 15\%$ (dashed line). The inner curve (dash-dot) is obtained by fixing h and using the 30% prior on M_1 .

D. The $\sigma_8 - \Omega_m$ Plane

We have seen it is impossible to obtain information about Ω_m and M_1 simultaneously due to a degeneracy of the form $\Omega_m/M_1 = \text{constant}$. For our fiducial model, we saw in particular that M_1 and Ω_m satisfy $\Omega_m/M_1 = (5.0^{+4.8}_{-2.5}) \cdot 10^{-14} M_\odot^{-1}$ (95% confidence). The fact that Ω_m/M_1 is so poorly constrained is reflected in the constraints one may obtain on Ω_m when assuming priors on M_1 and vice-versa. It seems then that local cluster abundances are not well suited to constrain either Ω_m or M_1 .

Up to date, most of the work on cluster abundances has been aimed at providing confidence regions in the $\sigma_8 - \Omega_m$ plane (see e.g. [40],[53],[1], [24] and references therein). It is helpful then to study the type of constraints we can place in the $\Omega_m - \sigma_8$ plane, not only to touch base with other work in this area, but also to see whether we can indeed expect to constrain cosmology with local cluster surveys.

We show in figure 5 our constraints, where we plot the 95% confidence regions in the $\Omega_m - \sigma_8$ plane for various gaussian priors on M_1 (marginalization over all other parameters is also done just as before). The dotted line is for a gaussian prior with $\Delta M_1 = 50\%$, the solid line is for $\Delta M_1 = 30\%$, and the dashed line for $\Delta M_1 = 15\%$. The most strongly constrained combination of σ_8 and Ω_m using a 30% prior on M_1 is $\sigma_8 \Omega_m^{0.13} \approx \text{const}$. Notice this constraint is rather different from the one typically found in the literature from local cluster abundances, which looks more like $\sigma_8 \Omega_m^\gamma \approx \text{constant}$ with $\gamma \sim 0.5$. This is not surprising, however, given that there are major differences between our analysis and most previous treatments, including the use of clustering properties (bias), the probing of lower masses in the halo mass function, and a marginalization over h , which is often fixed in cluster abundance analysis. In light of this last point, we also plot in figure 5 the expected confidence region obtained when h is fixed and a 30% gaussian prior on M_1 is used (dash-dot curve). It should be evident that marginalization over h is extremely important, and that constraints derived by holding h fixed are over-optimistic.

The main point that should be very clear from figure 5 is that, because of the very strong $\Omega_m - M_1$ degeneracy, the constraints that we can place in Ω_m are entirely determined by how well can the amplitude of the mass-richness relation be calibrated. Further, we expect this to be a generic feature of all cluster abundance studies (regardless of the mass tracer used) since we believe the degeneracy stems from how the halo mass function scales with Ω_m .

E. Constraining Cosmology With Cluster Statistics

We have derived above the various constraints on the $\sigma_8 - \Omega_m$ plane that we expect to obtain from our model survey. Importantly, we saw that marginalization over h is necessary to avoid overly optimistic constraints. In light of this sensitivity to h , it seems worthwhile to determine what combination of σ_8 , Ω_m , and h is most strongly constrained by the data (assuming a prior calibration of α and M_1). We compute these combinations of parameters using a principal component analysis of the estimated correlation matrix. We find then that, for gaussian priors $\Delta M_1 = 30\%$ and

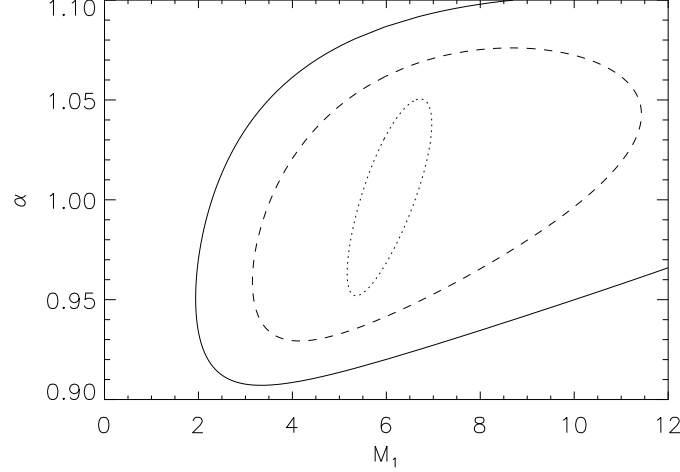


FIG. 6: The 95% confidence regions in the $\alpha - M_1$ plane. Moderate gaussian priors $\Delta m = \Delta n = \Delta h = 0.1$ and $\Delta \sigma_8 = 0.20$ were used for the solid line, while the dashed line uses $\Delta \Omega_m = \Delta n = \Delta h = 0.05$ and $\Delta \sigma_8 = 0.15$. The inner, dotted ellipse fixes cosmology. The 95% confidence regions for α when moderate priors are used is $\alpha = 1.000^{+0.081}_{-0.075}$. If one keeps cosmology fixed, M_1 can also be constrained, and the corresponding 95% confidence regions are $M_1 = 6.00^{+0.76}_{-0.68} \cdot 10^{12} M_\odot$ and $\alpha = 1.000^{+0.040}_{-0.039}$.

$\Delta \alpha = 10\%$ we can express the cosmological constraints (95% confidence level) as

$$\sigma_8 h^{-0.73} = 1.103^{+0.025}_{-0.025} \quad (45)$$

$$(\sigma_8 \Omega_m^{0.57})^{0.74} h = 0.374^{+0.133}_{-0.098} \quad (46)$$

$$\sigma_8^{-0.20} \Omega_m h^{-0.28} = 0.34^{+0.91}_{-0.25} \quad (47)$$

Not unexpectedly, the best constrained mode is mostly σ_8 , but with an important contribution from h (if this were not the case, marginalization over h would have had little effect before). We can see as well that Ω_m is the most poorly determined parameter, which makes sense given the large assumed uncertainty in M_1 and the strong $M_1 - \Omega_m$ degeneracy. The constraints on h that one can obtain with this method are at a moderately interesting level. If one introduces a prior $\Delta \Omega_m = 0.1$, the 68% confidence interval obtained from cluster statistics is $h = 0.7 \pm 0.09$, comparable to $h = 0.72 \pm 0.02 \pm 0.08$ from supernovae (Freedman et al. [19]) or $h = 0.72 \pm 0.05$ from the CMB (assuming a Λ CDM cosmology, see e.g. Spergel et al. [47]).

In view of the above comments, it is clear that aside from consistency checks, the most important contribution from local cluster statistics for the purposes of determining cosmological parameters is the accurate determination of σ_8 . In particular, using reasonable priors for all other variables we expect it will be possible to constrain σ_8 at the $\approx 10 - 15\%$ level with a 95% confidence level.¹⁵

F. Constraining the Halo Occupation Distribution

Let us consider now the complementary problem of constraining the halo occupation distribution by either fixing cosmology or marginalizing over it. These constraints should be of great interest in that they may help guide theoretical efforts in galaxy formation models. Our results are shown in figure 6, where we plot the 95% confidence regions on the $\alpha - M_1$ plane when we hold cosmology fixed (dotted line), marginalizing with strong gaussian priors $\Delta \Omega_m, \Delta n, \Delta h = 0.05$ and $\Delta \sigma_8 = 0.15$ (dashed line), and marginalizing over moderate priors $\Delta \Omega_m, \Delta n, \Delta h = 0.1$ and $\Delta \sigma_8 = 0.20$. As we expected, M_1 is poorly constrained and its confidence interval depends on the prior used in Ω_m . The slope α on the other hand, can be well constrained. Our moderate priors lead to a 95% confidence

¹⁵ By reasonable priors we mean $\Delta \alpha / \alpha = 10\%$, $\Delta M_1 / M_1 = 30\%$, $\Delta \Omega_m = 0.1$, $\Delta h = 0.1$, and $\Delta n = 0.1$.

Assumptions	$\Delta\alpha$	$\Delta\sigma_8$	Δh
$\Delta\Omega_m, \Delta n = 0.1$	± 0.038	± 0.079	± 0.089
$\Delta\Omega_m, \Delta n = 0.05$	± 0.032	± 0.048	± 0.070
$\Delta\Omega_m, \Delta n, \Delta h = 0.1$	± 0.036	± 0.080	-
$\Delta\Omega_m, \Delta n, \Delta h = 0.05$	± 0.028	± 0.037	-

TABLE I: $1 - \sigma$ predictions for α , σ_8 , and h from cluster samples obtained with SDSS type surveys. All error bars assume gaussian priors $\Delta\Omega_b h^2 = 0.002$, and $\Delta M_1 = 30\%$ as well as the assumptions listed on the table.

interval $\alpha = 1.000^{+0.081}_{-0.075}$. If one insists in keeping cosmology fixed, however, both α and M_1 may be constrained to a good accuracy. In particular, for fixed cosmology the 95% confidence regions become $\alpha = 1.000^{+0.040}_{-0.039}$ and $M_1 = 6.00^{+0.76}_{-0.68} \cdot 10^{12} M_\odot$.

G. What Do Local Cluster Abundances and Bias Tell us?

Given our above results, it seems fair to ponder as to what the best use of local cluster samples is. We have seen that bias allows us to constrain α and σ_8 simultaneously, though large degeneracies with h exist. We have also seen that cluster abundances and bias can only constrain the combination M_1/Ω_m , and only poorly at that. It seems then that rather than attempting to constrain cosmology alone or the mass tracer relations alone, the data is best used to constrain the three parameters α , σ_8 , and h .

We quote in table I how well can we constrain the various parameters (α , σ_8 , and h) under various assumptions. This is meant to illustrate the power of cluster samples obtained from SDSS type surveys. We assume in all cases gaussian priors $\Delta\Omega_b h^2 = 0.002$, and $\Delta M_1 = 30\%$. The values listed under the assumptions column are the values used as gaussian priors for the appropriate variable. All confidence intervals are 68% and marginalized over all other parameters.

Is this the best we can do? Yes and no. On the one hand, we can perform a singular value decomposition of the Fisher matrix assuming no priors on any of the parameters, thus determining which and how many directions are strongly constrained given our assumptions. We find that there are indeed three directions which may be strongly constrained, and these are most closely aligned to the α , σ_8 and h subspace. Thus, we cannot hope to place more than three strong constraints, and if we want to choose three of our parameters, our best choice is the triplet (α, σ_8, h) considered above. Nevertheless, the three directions which are most strongly constrained all have some contribution from the parameters M_1/Ω_m and n . In principle, then, we could do “better” if we opt for constraining combinations of the five parameters $(\alpha, \sigma_8, h, M_1/\Omega_m, n)$, though only three such combinations may be constrained.

VII. CLUSTER ABUNDANCES

A. The Role of Bias as a Complement to Cluster Abundances

We wish to consider now the type of constraints we can place if we have cluster abundance information alone. Before we do this, it is important to address whether the inclusion of clustering properties (in the form of cluster bias) contains information not included in the cluster richness function. If not, repeating our analysis disregarding bias information would not alter any of our results. We demonstrate that bias does indeed carry some additional information by considering how well can α be determined from our data.

Figure 7 shows the 95% confidence regions in the $\alpha - \sigma_8$ plane, marginalized over all other parameters, and where in addition to the usual priors on h, n , and Ω_b we used priors $\Delta M_1 = 30\%$ and $\Delta\Omega_m = 0.1$. The solid lines are obtained by using cluster abundances but ignoring bias, while the dotted lines are obtained by ignoring cluster abundances but including bias. Also shown as a dashed ellipse is the curve we obtain when both bias and abundances are used. Note this last ellipse is the same as the dashed ellipses in figure 4. The important result then is that cluster abundances are degenerate in $\alpha - \sigma_8$ ($\alpha\sigma_8^{0.47} \approx \text{constant}$) while bias breaks this degeneracy. This demonstrates explicitly that information contained in the bias complements that of cluster abundances by themselves.

An important consequence of this argument is that, when bias information is not included, one needs to either fix α or assume some prior on it. We checked this explicitly by noting that the $\sigma_8 - \Omega_m$ confidence regions obtained from cluster abundance alone blow up if no prior is placed on α .

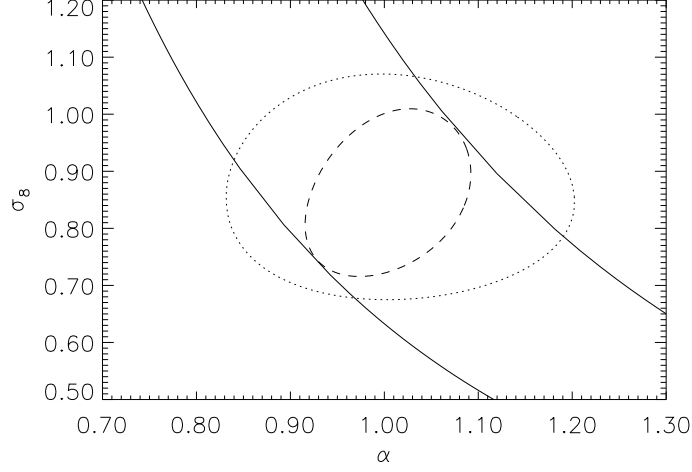


FIG. 7: The 95% confidence regions in the $\alpha - \sigma_8$ plane, marginalized over h, n, Ω_b, M_1 , and Ω_m with the usual priors on h, n , and Ω_b , and gaussian priors $\Delta M_1 = 30\%$ and $\Delta \Omega_m = 0.1$ for the last two parameters. The solid line is obtained when using cluster abundances but no bias information, while the dotted line corresponds to the converse case. We see that bias breaks an $\alpha - \sigma_8$ degeneracy which exits when using only cluster abundance information. Shown for comparison, the dashed ellipse above is the same as the dashed ellipse in figure 4, i.e. the confidence region obtained with both cluster abundance and bias information with the aforementioned priors on M_1 and σ_8 .

B. Can Local Cluster Abundance Alone Constrain σ_8 and Ω_m ?

In view of the degeneracy between α and σ_8 in cluster abundance considerations, we wish to consider to what extent the $\sigma_8 - \Omega_m$ plane can be constrained using cluster abundances alone. We have already seen that due to the $M_1 - \Omega_m$ degeneracy, the constraint on Ω_m is determined in its entirety by how well can the amplitude of the richness-mass relation be calibrated. Likewise, we expect that the constraints on σ_8 derived from cluster abundance studies to be entirely determined by the calibration constraints on α . This is shown explicitly in figure 8, where we plot the 95% confidence regions in the $\sigma_8 - \Omega_m$ plane for three different gaussian priors on α : $\Delta\alpha = 10\%$ (dotted line), $\Delta\alpha = 5\%$ (dash-dot), and $\alpha = \text{constant}$ (dashed line). A gaussian prior $\Delta M_1 = 30\%$ is used, and we marginalized over $\Omega_b h^2, n$, and h with the usual priors. When computing these confidence regions, we disregarded all bias information. Also shown for reference in the solid line is the contour obtained when both bias and cluster abundances are used and assuming a fixed α . We note that when including bias information, the confidence $\sigma_8 - \Omega_m$ region is not considerably worsened by letting α float (not shown).

It should be clear from figure 8 that, as we expected, the σ_8 confidence interval is entirely determined by the prior on α , just as the Ω_m interval is determined by the M_1 prior. Further, we note that the constraints on σ_8 are rather weak for realistic priors on α . In particular, even when all parameters except α and σ_8 are fixed, the 95% confidence interval assuming gaussian priors $\Delta\alpha = 10\%$ and $\Delta\alpha = 5\%$ are $\sigma_8 = 0.85^{+0.38}_{-0.26}$ and $\sigma_8 = 0.85^{+0.19}_{-0.15}$ respectively.

There are thus two main results from this exercise. Firstly, cosmology can be constrained by optical cluster abundances only to the extent that a careful calibration of the richness-mass relation can be achieved. Secondly, we find that using realistic assumptions for the accuracy of the calibration parameters neither σ_8 nor Ω_m may be accurately constrained by cluster abundances alone. As a corollary, it is evident that any constraints placed on Ω_m and σ_8 using cluster abundances which are not properly marginalized over M_1 and α will lead to overly optimistic constraints (see figure 11).

C. What do Local Cluster Abundances Alone Tell Us?

As in section VI G, we can now ask ourselves how we can best use cluster abundance information. We attack this question by finding the eigenvalues and eigenvectors of the estimated parameter correlation matrix. Upon doing so, we see that there are only two directions which are strongly constrained. These two eigenvectors are most closely aligned with the $(\alpha\sigma_8^{0.5} - h)$ plane, but have contributions from Ω_m/M_1 and n , as well as a very weak contribution

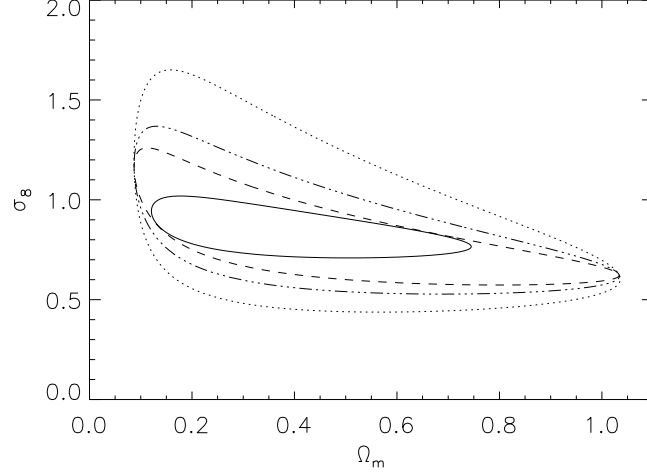


FIG. 8: The 95% confidence regions above are obtained using gaussian priors on Ω_b , n , and h , and disregarding all bias information. i.e. these are the expected confidence regions from optical cluster abundance studies. Note in particular the scale on the σ_8 axis. The various curves correspond to different priors on the richness-mass relation parameters. These are $\Delta\alpha/\alpha = 10\%$ (dotted), $\Delta\alpha/\alpha = 5\%$ (dash-dot), and $\Delta\alpha = 0$ (dashed). All contours are obtained using a 30% gaussian prior on M_1 . For comparison, we also show the contour obtained when we add bias information and keep α fixed, shown here in the solid line. Compare also to figure 5 (though note the change in scale for the σ_8 axis).

from σ_8 . For reference, we write the eigenvectors below¹⁶

$$\alpha \left(\sigma_8 (\Omega_m/M_1)^{0.73} \right)^{0.5} h^{0.51} + 0.15\delta n \quad (48)$$

$$(\alpha \sigma_8^{0.50})^{0.66} (\Omega_m/M_1)^{-0.23} h^{-1} - 0.39\delta n \quad (49)$$

where $n = 1 + \delta n$. Though these may not seem terribly illuminating, these expressions contain much information. Consider the first eigenvector: if we take all parameters except σ_8 and Ω_m to be fixed, this eigenvector reduces to $\sigma_8 \Omega_m^{0.73} = \text{constant}$, a cluster normalization condition. Thus, equation 48 may be thought of as a generalized cluster abundance normalization condition (see Appendix A for more discussion).

The second eigenvector above, equation 49, does not have a simple interpretation (though see Appendix A). Regardless, there are still elements which are of interest. Importantly, only the combinations Ω_m/M_1 and $\alpha \sigma_8^{0.5}$ appear, which are the degeneracies we have already found. This confirms that this degeneracies are indeed intrinsic to cluster abundance studies and cannot be avoided.

As a final note and in answer to the question posed by the title of this section, we state here that cluster abundances are most well suited to constrain the combination $\alpha \sigma_8^{0.50}$ and h . The constraints are somewhat sensitive to n and Ω_m/M_1 , but only moderately so. We show in table II the 68% confidence intervals for $\alpha \sigma_8^{0.50}$ under various assumptions.

D. Origin of the Degeneracies

Perhaps the most surprising result so far is that local cluster abundances alone are not capable of constraining either Ω_m or σ_8 very precisely when using reasonable priors for the richness-mass relation. This result, however, was obtained for optical cluster surveys, which amounts operationally to a choice of mass scale M_1 and power law index α in the scaling of the mass tracer with halo mass. It is possible then that our conclusions do not hold in the case of X-ray surveys or other mass tracers, where one would have different values for M_1 and α . Here, we wish to investigate

¹⁶ In these expressions we have disregarded the very weak dependence on σ_8 alone. This dependence shows up as an extra factor of $\sigma_8^{0.03}$ in both eigenvectors

Assumptions	$\Delta\alpha\sigma_8^{0.5}$
	0.090
$\Delta\alpha = 10\%$	0.074
$\Delta\alpha = 10\%, \Delta\sigma_8 = 0.2$	0.064
$\Delta\alpha = 10\%, \Delta\sigma_8 = 0.2, \Delta h = 0.1$	0.050
*	0.053
* + $\Delta h = 0.05$	0.035

TABLE II: $1 - \sigma$ predictions for $\alpha\sigma_8^{0.5}$ from cluster samples obtained with SDSS type surveys. All error bars assume gaussian priors $\Delta\Omega_b h^2 = 0.002$, $\Delta M_1 = 30\%$, $\Delta n = 0.1$, and $\Delta\Omega_m = 0.1$, as well as the assumptions listed on the table. The next to last row, marked with a * in assumptions, assumes $\Delta\Omega_m = 0.05$ and $\Delta n = 0.05$, as well as priors $\Delta\alpha = 10\%$ and $\Delta\sigma_8 = 0.2$. In all cases where no prior on h is assumed, the $1 - \sigma$ interval for h is $h = 0.7 \pm 0.1$, which reduces to $h = 0.70 \pm 0.08$ for case *.

where the degeneracies stem from to determine whether we expect them to be generic or particular to the fiducial model we have assumed.

1. $M_1 - \Omega_m$ Degeneracy

Let us begin by analyzing the $M_1 - \Omega_m$ degeneracy first. We concluded in section VIB that as long as the mass tracer scales with mass as some function of m/M_1 for some characteristic mass scale M_1 , then the degeneracy between M_1 and Ω_m will always exist. The only possible way out of this statement is that our starting assumption, namely equation 41, is violated. We discuss then what conditions equation 41 imposes on the mass function.

Let us assume that equation 41 holds and consider the product $dx f(x)$ for two values (m, Ω_m) and (m', Ω'_m) . Equation 41 implies

$$dm \bar{n}(m, \Omega_m) = dm' \bar{n}(m', \Omega'_m) \quad (50)$$

provided $m'/\Omega'_m = m/\Omega_m$. Defining $\lambda \equiv \Omega'_m/\Omega_m$, we obtain $m' = \lambda m$, which upon replacing on the right hand side above yields

$$dm \bar{n}(m, \Omega_m) = dm \lambda \bar{n}(\lambda m, \lambda \Omega_m). \quad (51)$$

In other words, equation 41 holds if and only if the halo mass function satisfies the scaling relation¹⁷

$$\bar{n}(m, \Omega_m) = \lambda \bar{n}(\lambda m, \lambda \Omega_m). \quad (52)$$

Letting $\Omega_m = 1$, this relation simplifies to

$$\bar{n}(m)|_{\Omega_m=1} = \Omega_m \bar{n}(\Omega_m m, \Omega_m). \quad (53)$$

which was indeed found by Zheng et al. [57] using extensive numerical simulations. In fact, they found the correlation function scales in a similar way, supporting the fact that the $M_1 - \Omega_m$ degeneracy we found is not broken when bias is included as an additional observable.

We are forced to conclude then that there is an intrinsic limit to how well can we constrain Ω_m from cluster abundances which is set by the uncertainty in the characteristic mass scale M_1 . Mass measurements at present are only accurate to about 20% (optimistically) to 50% (pessimistically), which essentially sets the maximum accuracy one could achieve in Ω_m using local cluster surveys. Note, however, that we found that the ratio M_1/Ω_m itself was rather poorly constrained, so it seems unlikely that local cluster abundances can provide strong constraints on Ω_m .¹⁸

¹⁷ The converse is proved simply by reversing our argument.

¹⁸ Note we are not making any such claim for cluster abundance studies extending over a large redshift range, since then it is possible to provide constraints using the observed growth of structure.

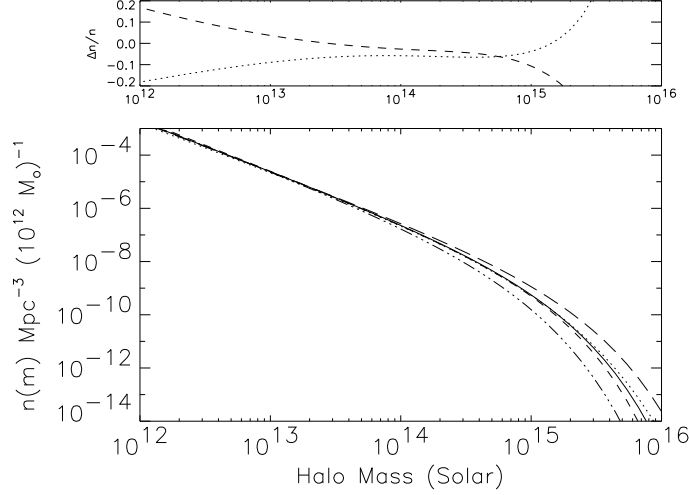


FIG. 9: Shown above in the solid line is the Sheth Tormen halo mass function for our fiducial model ($\sigma_8 = 0.85$). Also shown are the scaled mass functions (i.e. right hand side of equation 57) for $\sigma'_8 = 1.0$ (dashed line) and $\sigma'_8 = 0.7$ (dotted line). For comparison, we also show the unscaled halo mass functions for $\sigma_8 = 1.0$ and $\sigma_8 = 0.7$ with the long-dash and dash-triple dot lines respectively. The scaled mass functions are seen to agree with each other to within $\approx 10\%$ or better in the mass range $10^{12} - 10^{15} M_\odot$. The difference between the scaled mass function and our fiducial model mass function, divided by the halo mass function, is shown in the upper panel. Conventions are the same: $\sigma'_8 = 1.0$ corresponds to the dashed line while $\sigma'_8 = 0.7$ is shown with the dotted line.

2. $\alpha - \sigma_8$ Degeneracy

Let us now turn to the $\alpha - \sigma_8$ degeneracy. We perform an analysis similar to the one above to determine if the degeneracy stems from a scaling property of the halo mass function.

Consider then a variation of $(\alpha, \sigma_8) \rightarrow (\alpha', \sigma'_8)$ which leaves cluster abundances fixed. The relation between the parameters is easily obtained from a singular value decomposition of the Fisher matrix holding all parameters fixed except for α and σ_8 . We obtain that cluster abundances are approximately degenerate when $\alpha \sigma_8^{0.5} = \alpha' \sigma_8'^{0.5}$.

Now, since our mass tracer scales with mass as a power law, the binning functions may be expressed in terms of a function $g(\alpha \ln(m/M_1))$. We have then

$$N_{\bar{a}}(\alpha', \sigma'_8) \propto \int dm' \bar{n}(m', \sigma'_8) g(\alpha' \ln(m'/M_1)). \quad (54)$$

We perform now a change of variables by defining m via $\alpha \ln(m/M_1) = \alpha' \ln(m'/M_1)$. Defining $\lambda = \alpha/\alpha'$ and replacing above we get

$$N_{\bar{a}}(\alpha', \sigma'_8) \propto \int dm \lambda (m/M_1)^{\lambda-1} \bar{n}(m', \sigma'_8) g(\alpha \ln(m/M_1)) \quad (55)$$

which is to be compared with

$$N_{\bar{a}}(\alpha, \sigma_8) \propto \int dm \bar{n}(m, \sigma_8) g(\alpha \ln(m/M_1)). \quad (56)$$

If we demand that $\sigma'_8 = \lambda^2 \sigma_8$, we have then that $\alpha \sigma_8^{0.5} = \alpha' \sigma_8'^{0.5}$, and thus by construction $N_{\bar{a}}(\alpha, \sigma_8) \approx N_{\bar{a}}(\alpha', \sigma'_8)$. Since the function g is the same in both equations 55 and 56, this suggests that the kernel of the integrals are nearly degenerate. We thus make the ansatz

$$\bar{n}(m, \sigma_8) \approx \lambda \left(\frac{m}{M_1} \right)^{\lambda-1} \bar{n}(M_1 (m/M_1)^\lambda, \lambda^2 \sigma_8). \quad (57)$$

We check our ansatz using the Sheth-Tormen halo mass function. In particular, figure 9 shows the Sheth-Tormen halo mass function, computed for our fiducial model, as well as the scaled mass functions computed according to

equation 57. The smaller plot above shows the fractional difference between the right and left hand sides of equation 57. The right hand side of equation 57 was computed for $\sigma'_8 = 1.0$ (dashed line) and $\sigma'_8 = 0.7$ (dotted line). We find that our scaling relations are accurate to within $\approx 10\%$ for σ_8 in the range $[0.7, 1.0]$ and over the mass range $10^{13}M_\odot - 10^{15}M_\odot$. Even though the accuracy of the scaling relations decreases as we move away from this range, it is still better than 20% from $10^{12}M_\odot$ up to $\approx 2 \cdot 10^{15}M_\odot$ for σ_8 in the range $0.7 < \sigma_8 < 1.0$.

We conclude therefore that, in the mass ranges probed by our model, there appears to exist a scaling relation given by equation 57. Further, running the argument we used to derive our ansatz in reverse proves that the degeneracy we observe does indeed stem from the scaling relation 57. We thus expect our results to hold for all mass tracers that scale with mass via a power law and which probe the mass range $10^{13} - 10^{15}M_\odot$. In particular, we expect a degeneracy between α and σ_8 to exist for all cases (though recall bias breaks this degeneracy) as well as an $M_1 - \Omega_m$ degeneracy. This further implies that any determination of cosmological parameters done using local cluster abundances alone needs to be marginalized over uncertainties in how the mass tracer scales with mass, regardless of the choice of mass tracer. Note marginalization over the hubble rate is also necessary due to large mixing between the cosmological parameters for fixed cluster densities.

To close, we note the fact that the scaling relation 57 depends on M_1 . This suggests that a more accurate degeneracy can be achieved by allowing M_1/Ω_m to vary using for example equations 48 and 49. Nevertheless, the relation we obtained works well, and is only weakly dependent on the value of M_1 . Indeed, we can change M_1 by up to a factor of two up or down and still get a reasonable agreement in the scaling relation 57. It is likely therefore that the role of M_1 is essentially to set the mass scale over which the halo mass function will satisfy scalings of the form 57.

VIII. CONCLUSIONS

We have derived expressions for cluster abundances and bias using the halo model formalism. In particular, we have shown how starting from the halo mass function and halo bias, we can obtain expressions for cluster statistics in terms of any mass tracer (e.g. X-ray temperature/luminosity, number of galaxies, etc.) in such a way that various experimental effects can be included in the formalism. Specifically, we include intrinsic dispersion of the richness-mass relation, bias and/or scatter due to experimental measurements, detection rates, and false detections. We also identified various sources of errors and derived the uncertainties one expects due to intrinsic scatter in the richness-mass relation. We believe that these derivations are important in that they allow us to compare theory directly to observations, without having to manipulate the observations in attempts to retrieve, for instance, the halo mass function. Further, they allow us to consider the possibility of using cluster statistics to constrain not just cosmology, but also how the mass tracer scales with halo mass.

Having derived our formalism, we applied it to the case of large local optical cluster surveys. In this context, we have shown that optical cluster survey determinations of cluster abundances and bias can provide strong constraints on the amplitude of the power spectrum at cluster scales (σ_8), the power law index on the scaling relation of the number of galaxies in a halo of mass m , and perhaps even the hubble parameter h (see table I). We argued as well that cluster abundances and bias are not well suited for constraining Ω_m or M_1 , the amplitude of the mass tracer scaling relation with mass.

We have shown as well that one needs to be very careful when analyzing cluster abundances and bias data in order to avoid overly optimistic constraints. In particular, we have shown that realistic constraints on σ_8 need to be marginalized over h and, when bias information is unavailable, marginalization over priors on α is also necessary. Though marginalization over M_1 has a much smaller effect on σ_8 , it becomes of paramount importance if one wishes to constrain Ω_m . In fact, we found that the uncertainties in σ_8 and Ω_m obtained from cluster abundance studies alone are entirely determined by the priors used on α and M_1 .

We have attempted to explain why is it that the uncertainties in σ_8 and Ω_m are driven by the priors on α and Ω_m when only cluster abundance information is used. In particular, we have argued that this effect is driven by two degeneracies, one involving M_1 and Ω_m , the other involving α and σ_8 . We have shown here that these degeneracies arise from scaling laws satisfied by the halo mass functions. The scaling law leading to the $M_1 - \Omega_m$ degeneracy was found empirically by Zheng et al. [57], but it is reassuring to see it re-emerge here in our Fisher analysis. The scaling law 57 leading to the $\alpha - \sigma_8$ degeneracy is, to the best of our knowledge, a new result.

Finally, we argued that because the degeneracies above stem from intrinsic scaling relations of the halo mass function, our conclusions are valid for any cluster abundance study in which the mass tracer scales with mass as a power law to a good approximation. In particular, for any such studies, any constraints that one wishes to place on cosmology need to be properly marginalized over the hubble rate h as well as the amplitude and power law index of the mass tracer scaling relation.

In summary, then, we have found that cluster abundances and cluster bias are powerful tools that can greatly constrain both the amplitude of the power spectrum at cluster scales, and how the number of galaxies in a halo scales

with mass. However, neither Ω_m nor the characteristic mass scale for the formation of galaxies can be accurately constrained. In either case, it is always important to marginalize over h in order to avoid obtaining unrealistically tight constraints.

IX. ACKNOWLEDGMENTS

We would like to thank Andrey Kravtsov, Andreas Berlind, Risa Wechsler, and James Annis for helpful comments and discussion. We would also like to thank our referee for useful comments which greatly improved our presentation. This work was carried out at the University of Chicago, Center for Cosmological Physics and was supported in part by NSF PHY-0114422 and NSF Grant PHY-0079251.

-
- [1] Allen, S.W., Schmidt, R.W., Fabian, A.C. and Ebeling, H. MNRAS **342**, 287 (2003).
 - [2] Annis, J. et al. In preparation.
 - [3] Bahcall, N.A. astro-ph/9901076v1.
 - [4] Bahcall, N.A. et al. ApJ **585**, 182 (2003) .
 - [5] Bahcall et al. astro-ph/0305202.
 - [6] Benson, A.J., Cole, S., Frenk, C.S., Baugh, C.M., & Lacey, C.G. astro-ph/9903343
 - [7] Beranardeau, F. et al. astro-ph/0112551.
 - [8] Berlind, A.A., & Weinberg, D.H. astro-ph/0109001
 - [9] Berlind et al. astro-ph/0212357.
 - [10] Blanton, M.R. et al. AJ **121**, 2358 (2001) .
 - [11] Borgani, S. & Guzzo, L. Nature **409**, 39 (2001).
 - [12] Carlstorm, J.E., Holder, G.P., & Reese, E.D. Ann. Rev. A.& A. **40**, 463 (2002).
 - [13] Colless, M. et al. MNRAS **328**, 1039 (2001).
 - [14] Cooray, A. ApJ **576**, 105 (2002) .
 - [15] Cooray, A., & Sheth, Ravi. astro-ph/0206508.
 - [16] Dodelson, S. *Modern Cosmology*. Academic Press, 2003.
 - [17] Evrard, A.E. et al. ApJ **573**, 7 (2002) .
 - [18] Feldman, H.A., Kaiser, N., and Peacock, J.A. ApJ **426**, 23 (1994) .
 - [19] Freedman, W.L. ApJ **553**, 47 (2001) .
 - [20] Goto, T. et al. AJ **123**, 1807 (2002) .
 - [21] Hu, W., and Eisenstein, D. ApJ **496**, 605 (1998) .
 - [22] Hu, W. and Kravtsov, A.V. astro-ph/0203169.
 - [23] Huchra, J.P. and Geller, M.J. ApJ **257**, 423 (1982) .
 - [24] Ikebe, Y. et al. A& A **383**, 773 (2002).
 - [25] Jarvis, M. et al. AJ **125**, 1014 (2003) .
 - [26] Jenkins et al. MNRAS **321**, 372 (2001).
 - [27] Jing, Y.P., Mo, H.J., and Börner, G. ApJ **494**, 1 (1998)
 - [28] Kim, R.S.J. et al. AJ **123**, 20 (2002) .
 - [29] Kochanek, C.S. et al. ApJ **202**, 1112 (2003) .
 - [30] Kochanek, C.S. et al. ApJ **585**, 161 (2003) .
 - [31] Kravtsov et al. astro-ph/0308519
 - [32] Lemson, G. & Kauffmann, G. MNRAS **286**, 795 (1997)
 - [33] Magliocchetti, M. and Porciani, C. astro-ph/0304003.
 - [34] Moore, B., Quinn, T., Governato, F., Stadel, J., & Lake, G. MNRAS **310**, 1147 (1999).
 - [35] Moustakas, L.A. and Somerville, R.S. ApJ **577**, 1 (2002) .
 - [36] Navarro, J., Frenk, C., & White, S.D.M. ApJ **462**, 563 (1996) .
 - [37] Nichol, R.C. astro-ph/0305041.
 - [38] Nichol, R.C. et al. Mining the Sky, 213 (2001).
 - [39] Pierpaoli, E., Scott, D., & White, M. MNRAS **325**, 77 (2001).
 - [40] Pierpaoli, E. et al. MNRAS **342**, 163 (2003).
 - [41] Press, W.H., Schechter, P. ApJ **187**, 425 (1974)
 - [42] Seljak, U. MNRAS **337**, 769 (2002).
 - [43] Sheth, R.K., & Tormen, G. MNRAS **308**, 119 (1999)
 - [44] Scherrer, R.J. & Weinberg, D.H. ApJ **304**, 607 (1998) .
 - [45] Schuecker, P. et al. A& A **398**, 867 (2003)
 - [46] Scoccimarro, R., Sheth, R.K., Hui, L., and Jain, B. ApJ **546**, 20 (2001)
 - [47] Spergel et al. ApJ **148**, 175 (2003) .

- [48] Tadros, H., Efstathiou, G., Dalton, astro-ph/9708259.
- [49] Tegmark, M. et al. ApJ **499**, 555 (1998) .
- [50] Thomas, P.A. MNRAS **330**, 48 (2002).
- [51] van den Bosch, F.C., Mo, H.J., and Yang, Xiaohu. MNRAS **345**, 923 (2003)
- [52] Viana, P.T.P., & Liddle, A.R. MNRAS **281**, 323 (1996).
- [53] Viana, P.T.P. et al. MNRAS **346**, 319 (2003).
- [54] Yang, Xiaohu, Mo, H.J., and van den Bosch, F.C. MNRAS **339**, 1057 (2003)
- [55] York, D.G. et al. ApJ **571**, 172 (2002) .
- [56] Zehavi, I. et al. astro-ph/0301280.
- [57] Zheng, Z. et al. astro-ph/0202358.

APPENDIX A: WHERE DID THE USUAL $\sigma_8 - \Omega_m$ DEGENERACY GO?

Cosmological constraints from cluster abundance studies are usually expressed in the form of the so called cluster abundance normalization condition, usually expressed as $\sigma_8 \Omega_m^\gamma \approx 0.5$ where $\gamma \approx 0.5$. In other words, cluster abundances are usually used to constrain the combination $\sigma_8 \Omega_m^\gamma$. This combination of parameters, however, did not arise from our analysis. Where did the usual $\sigma_8 - \Omega_m$ degeneracy go?

1. The $\sigma_8 - \Omega_m$ Degeneracy

Let us consider first equation 48. We stated in section VII C that 48 could be thought of a generalized cluster abundance normalization condition. While the exponent of Ω_m is a little steeper than usual, we show below that this arises simply because we are probing rather low mass scales.

We begin our analysis by determining the 95% confidence regions in the $\sigma_8 - \Omega_m$ plane obtained using only our 10 richest bins (clusters having 35 galaxies or $M \gtrsim 2 \cdot 10^{14} M_\odot$) while holding all parameters except σ_8 and Ω_m constant. This is shown in figure 10 with a dotted line. The degeneracy axis in the figure is $\sigma_8 \Omega_m^{0.62} = \text{constant}$, so we see then that we do indeed recover the cluster normalization condition when, a- we hold all other parameters fixed, and b- restrict ourselves to the most massive clusters. This degeneracy simply reflects the fact that the halo mass function at $m \sim 10^{14} M_\odot$ scales is degenerate according to the above expression (see e.g. Zheng et al. [57]). On this basis, one would expect that probing low mass scales would allow us to break this degeneracy, which is indeed the case. We show this in figure 10 where we plot the confidence regions obtained when including lower mass clusters. In particular, the confidence regions shown with the dashed and solid lines in figure 10 are obtained using all but the lowest six bins ($N_{gal} > 21$ or $M \gtrsim 10^{14} M_\odot$) and all bins respectively. We see that with the inclusion of lower mass bins the degeneracy region is greatly reduced. Further, as we probe lower and lower masses, the axis which is least strongly constrained becomes steeper and steeper, going from 0.62 when only the 10 richest bins are used to 0.73 when all bins are used.

We can gain further insight on the $\sigma_8 - \Omega_m$ degeneracy by considering what happens when we allow M_1 and α to vary, but keeping h fixed. The two most constrained directions are obtained from the estimated parameter correlation matrix are¹⁹

$$\alpha \left(\sigma_8 (\Omega_m / M_1)^{0.67} \right)^{0.50} = 0.503 \cdot 10^{-12} M_\odot^{-1} \pm 2\% \quad (\text{A1})$$

$$\alpha^{0.32} (\Omega_m / M_1)^{-1} = 20.0 \cdot 10^{12} M_\odot \pm 13\%. \quad (\text{A2})$$

Note that these two eigenvectors are *not* simply expressions 48 and 49 with h held constant. To see how they are related, it is best to pretend we know nothing about equations 48 and 49 while we analyze the above eigenvectors. We can then go back and see how the pair of eigenvectors 48 and 49 are related to A1 and A2.

Let us then analyze the above eigenvectors, whose structure allows for a very simple interpretation. Take α and M_1 to be fixed. Then, the first eigenvector becomes the cluster normalization condition $\sigma_8 \Omega_m^{0.67}$, while the second eigenvector is almost entirely Ω_m . Since the low mass end of the halo mass function is essentially independent of Ω_m , this suggests the first eigenvector is driven by the high mass end of the halo mass function only, while the second eigenvector is driven by the low mass end alone. Indeed, the eigenvectors obtained when restricting ourselves to high

¹⁹ We are again neglecting a small dependence on σ_8 of the form $\sigma_8^{0.3}$ in equation A2.

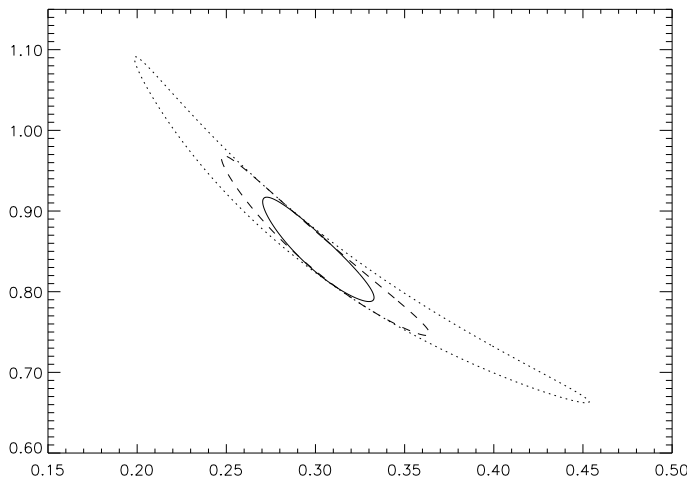


FIG. 10: The figure above shows two things: first, that when we restrict our analysis to σ_8 and Ω_m holding all other parameters fixed, and considering only massive clusters ($N_{gal} \geq 35$) we recover the usual $\sigma_8 - \Omega_m$ degeneracy (dotted line, 95% confidence). Also shown are the 95% confidence regions obtained using all but the lowest six bins (dashed) and all bins (solid). This illustrates the fact that probing low halo masses breaks the $\sigma_8 - \Omega_m$ degeneracy by a considerable amount. Therefore, we do not expect to recover the usual cluster normalization condition since we are probing rather low halo masses.

mass bins (clusters with 35 galaxies or more) are close to those above, except that we do not lose any constraining power for the first eigenvector, while the constraint on the second eigenvector is weakened by a factor of four. We conclude then that equation A1 may be thought of as the constraint arising from matching the high mass end of the halo mass function, while equation A2 arises from matching the low mass end.

Are the vectors A1 and A2 related to the vectors we found in section VII C? To approach this question, we can consider what happens to the vectors A1 and A2 when we let h vary.

Consider first what happens at a qualitative level: h affects both the high mass end and the low mass end of the halo mass function. As such, we do not expect our eigenvectors to cleanly separate into matching one or the other end of the halo mass functions- they will mix. Indeed, when we let h vary, the first eigenvector becomes

$$\alpha \left(\sigma_8 (\Omega_m / M_1)^\gamma \right)^{0.50} h^{\tilde{\gamma}} = \text{constant} \quad (\text{A3})$$

where γ and $\tilde{\gamma}$ depend on the lowest mass scale probed. e.g. $\gamma = 0.73$ when all bins are used (as we found in section VII C) while $\gamma = 0.62$ when we use only rich clusters.

We note several things: first, the vector A3 is essentially identical to 48 when n is held fixed. Interestingly, though, the $\sigma_8 \Omega_m^\gamma$ degeneracy no longer has the constant exponent $\gamma \approx 0.62$. The variation of the exponent comes about because of the mixing of the constraints from the low and high mass ends of the halo mass function, and hence our result above compromises by giving us the most strongly constrained direction in the $\sigma_8 - \Omega_m$ plane when all other parameters are held fixed.

What about the eigenvector from expression A2? Since h mixes the high and low mass end constraints, one may expect the eigenvector A2 not only to be drastically altered (since it no longer represent the low mass end constraint), but also to be greatly weakened since the constraining power of the high and low mass ends of the halo mass function now goes into the first eigenvector. This is indeed the case. Despite this result, however, there is still a second highly constrained eigenvector, which is essentially that of expression 49 with n fixed. This eigenvector is a new constraint that arises from allowing h to vary, and is thus not associated with the eigenvector from expression A2.

2. Hiding the $\sigma_8 - \Omega_m$ Degeneracy

We argued throughout the text that the appearance of the $\alpha - \sigma_8$ and $M_1 - \Omega_m$ degeneracies makes marginalization over the mass tracer scaling relation necessary if one wishes to avoid placing overly optimistic constraints on the cosmological parameters. A by product of this marginalization is that the characteristic shape of the $\sigma_8 - \Omega_m$

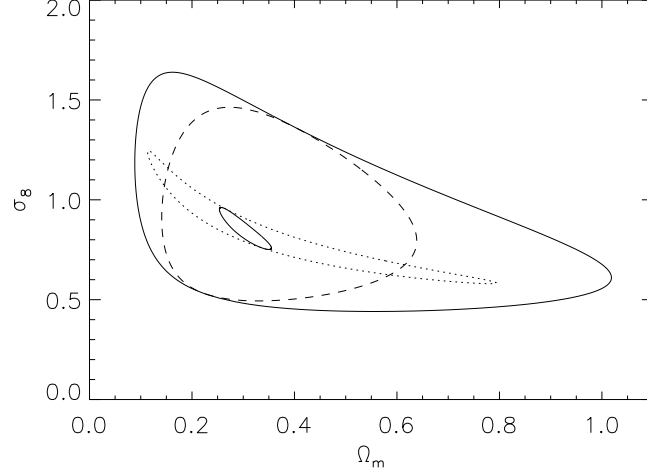


FIG. 11: The effect of allowing various parameters to vary in determining the $\sigma_8 - \Omega_m$ confidence regions is shown above. All curves above are 95% confidence and hold n and $\Omega_b h^2$ fixed. The inner solid curve also holds α , M_1 , and h fixed. The dashed curve allows α and M_1 to vary with priors $\Delta\alpha/\alpha = 10\%$ and $\Delta M_1/M_1 = 30\%$. The dotted curve holds α and M_1 fixed, but varies h with the prior $\Delta h = 0.1$. Finally, the outer solid curve allows α , M_1 , and h to vary with the aforementioned gaussian priors.

degeneracy is then completely washed out. We illustrate this effect below, not only to observe the degradation of the confidence regions, but also because we can get a better feel as to how important the various effects are.

We begin with the constraints on σ_8 and Ω_m when all other parameters are fixed. This is shown in figure 11 as the inner solid ellipse (95% confidence region), which matches that of figure 10. We now let α and M_1 to vary by assuming gaussian priors $\Delta\alpha/\alpha = 10\%$ and $\Delta M_1/M_1 = 30\%$. This is shown as a dashed curve in figure 11. The effect of allowing α and M_1 to vary is staggering- the confidence regions are enormously expanded.

We can likewise observe the effect of allowing h to vary while keeping the other parameters fixed. Figure 11 shows the 95% confidence regions (dotted line) marginalized over h with a gaussian prior $\Delta h = 0.1$. As we expect, one direction remains tightly constrained, corresponding to the eigenvector 49, the generalized cluster abundance normalization condition. On the other hand, the perpendicular direction is weakened to a large degree, again reflecting that a floating h mixes the high and low mass ends constraints from the halo mass function into a single constraint.

Finally, shown with the outer solid curve in figure 11 is the 95% confidence region when α , M_1 , and h are allowed to vary using the above priors. This last curve is the true constraint one may expect from cluster abundances alone. Also shown as reference with the thicker solid curve is the 95% confidence region obtained including bias information. All priors for this last curve are the same, except for α , for which no prior was assumed.